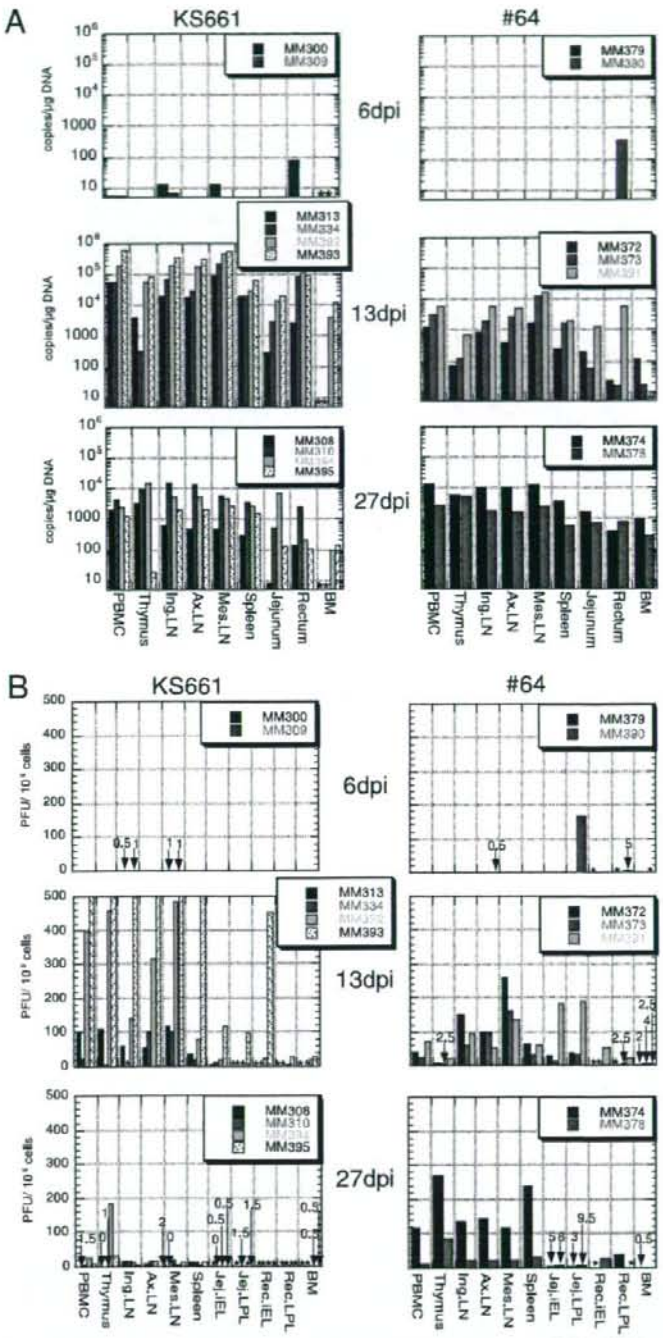

FIG. 2. (A) Proviral DNA loads in tissues of KS661- and #64-infected monkeys at 6, 13, and 27 dpi. Viral burdens were determined by quantitative PCR and expressed as the numbers of viral DNA copies per microgram of total DNA extracted from tissue homogenates. PBMC, peripheral blood mononuclear cells; Ing., inguinal; Ax., axillary; Mes., mesenteric; BM, bone marrow; *, not done. (B) Numbers of IVPCs in tissues of KS661- and #64-infected monkeys at 6, 13, and 27 dpi. Numbers of IVPCs were determined by an infectious plaque assay and were expressed as the numbers of PFU per 10^6 cells. Jej., jejunum; Rec., rectum; iEL, intraepithelial lymphocytes; *, not done.

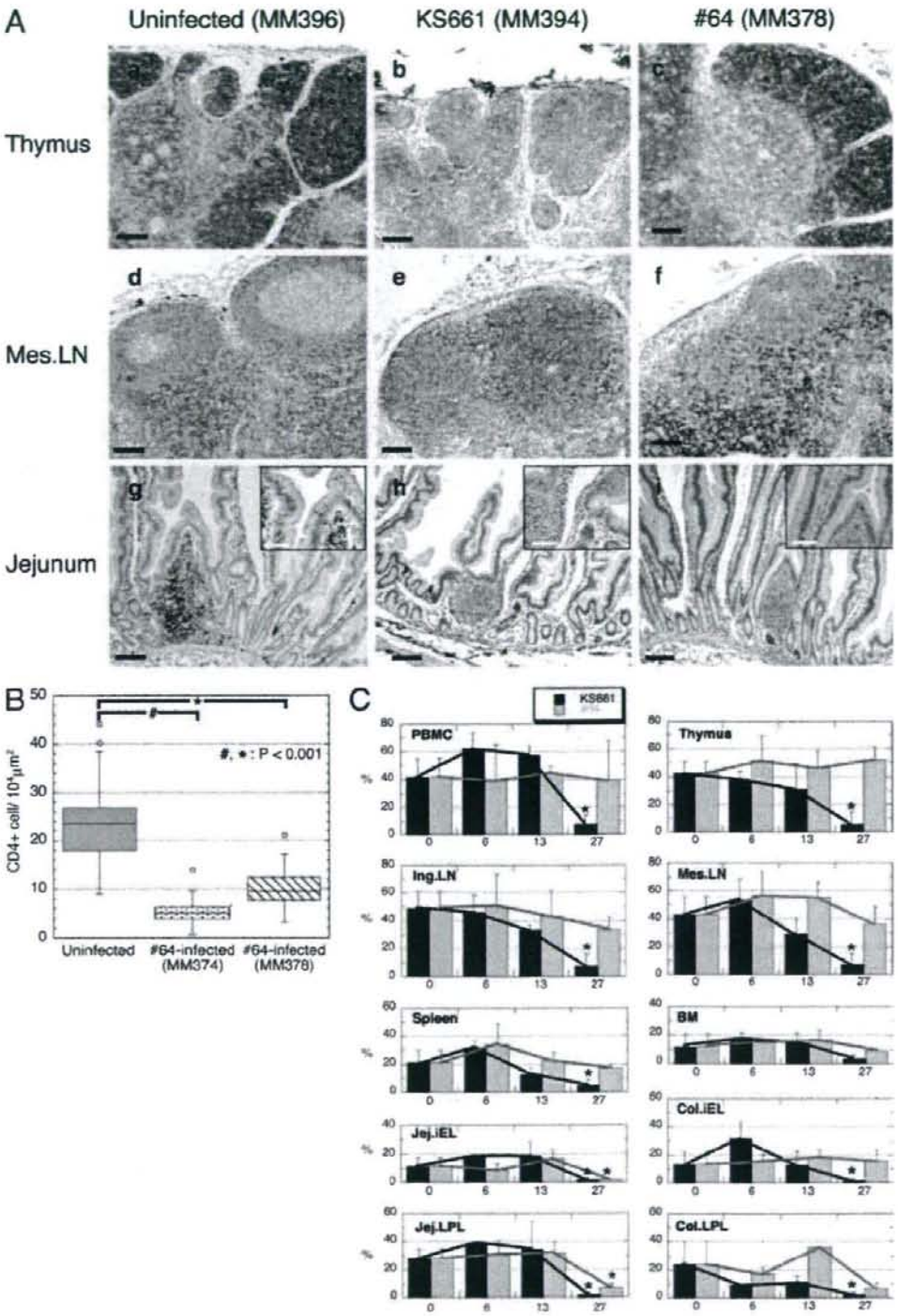

that in each sample from the KS661-infected monkeys. However, unlike the KS661 proviral DNA levels, the #64 proviral DNA levels in most tissues were maintained up to 27 dpi. These results suggest that #64 spread more slowly than KS661 and that the amounts of proviral DNA in a variety of tissues from the #64-infected animals were smaller than those in the tissues from KS661-infected animals around the initial peak of plasma viremia.

Because the amount of proviral DNA measured by PCR may include nonreplicating remnants of the viral genome, we also measured the number of IVPCs in each tissue sample by a plaque assay as described previously (9, 15). Briefly, cells prepared from infected animals were mixed with human T-lymphoid M8166 indicator cells, resuspended in culture medium containing 0.4% agarose, and plated into petri dishes. The plaques that formed in the cell layer were counted after 10 days of cultivation, and the number of IVPCs was calculated. For the KS661-infected monkeys, high numbers of IVPCs in all the tissue samples examined at 13 dpi were detected (Fig. 2B). Among these samples, the thymus and mesenteric LN samples harbored especially high numbers of IVPCs (more than 500/10^6 cells) at 13 dpi. The numbers of IVPCs declined remarkably from 13 to 27 dpi. We concluded that KS661 replicated systemically and synchronously in a variety of tissues, including the intestinal tract, at 13 dpi. In contrast, #64 production patterns in different tissues were not synchronous. Among #64-infected monkeys at 6 dpi, virus production was most active in the jejunum lamina propria lymphocytes (LPL) of MM390 (166 IVPCs/10^6 cells). At 13 dpi, interestingly, mesenteric LN became the center of virus production in two of the three monkeys examined (MM372 and MM373; 259 and 160 IVPCs/10^6 cells). In the other monkey (MM391), the jejunum had the highest number of IVPCs, followed by the mesenteric LN. These results suggested that the virus that replicated in the jejunum spread directly into the mesenteric LN via the flow of lymphatic fluid. At 27 dpi, the thymus tissues of both monkeys examined (MM374 and MM378) exhibited the highest numbers of IVPCs. In summary, the systemic dissemination of #64 was slower than that of KS661, and it was particularly delayed in the thymus during the acute phase.

Systemic $CD4^+$ cell depletion is the signature of disease induced by highly pathogenic SHIVs (7, 8, 22). We therefore compared the frequencies of $CD4^+$ cells in tissues from the animals infected with KS661 and #64, in addition to those of the circulating $CD4^+$ T lymphocytes. As representatives of the major virus-producing organs, the thymus, the mesenteric LN, and the jejunum were selected for examination. CD4 cell numbers were measured by immunohistochemistry analyses as described previously (18). Uninfected thymus tissue contained abundant $CD4^+$ cells that were stained brown (Fig. 3A, panel a), while the tissue collected from the KS661-infected animal at 27 dpi harbored few such cells (Fig. 3A, panel b). #64 caused virtually no $CD4^+$ cell depletion in the thymus at 27 dpi (Fig. 3A, panel c). In the mesenteric LN of uninfected monkeys, $CD4^+$ cells were found in the paracortical region (Fig. 3A, panel d). KS661 depleted $CD4^+$ cells in this area (Fig. 3A, panel e). Unlike KS661, #64 did not reduce the level of $CD4^+$ cells (Fig. 3A, panel f). The jejunum samples from uninfected animals contained $CD4^+$ cells in the lamina propria and follicles of gut-associated lymphatic tissues (Fig. 3 A, panel g). KS661 depleted $CD4^+$ cells in these tissues, too (Fig. 3A, panel h). Interestingly, #64 caused $CD4^+$ cell depletion in the small intestine comparable to that caused by KS661 (Fig. 3A, panel i). To confirm the observed cell reduction in the jejunum samples, we randomly selected a total of 40 fields on the tissue sections from each animal for viewing at a total magnification of ×400, counted $CD4^+$ cells, and averaged the numbers (Fig. 3B). The $CD4^+$ cell densities in the jejunum samples from the #64-infected monkeys were significantly lower than those in the samples from uninfected animals ($P < 0.001$). This gut-specific $CD4^+$ cell depletion caused by #64 prompted us to analyze the frequencies of $CD4^+$ T cells (including CD4 and CD8 doubly positive cells) in a variety of tissues by flow cytometry (Fig. 3C). KS661 caused systemic $CD4^+$ T-lymphocyte depletion by 27 dpi (Fig. 3C). In agreement with the immunohistochemistry results, #64 significantly depleted $CD4^+$ T cells only in the jejunum intraepithelial lymphocytes and LPL ($P = 0.01$ and 0.003, respectively) (Fig. 3C) by 27 dpi, although we examined only two #64-infected monkeys at 27 dpi. In conclusion, the $CD4^+$ T-cell depletion patterns caused by KS661 and #64 were distinct, and the small intestine was the only site in which $CD4^+$ T cells were significantly depleted by the moderately pathogenic #64.

Taken together, our results show that #64 disseminated more slowly and replicated less than KS661 in systemic lymphoid tissues, as well as in peripheral blood, during the acute phase of infection. We believe that because of its low rate and low levels of replication, #64 could not cause irreversible injury before the host mounted an immune reaction. As a result, $CD4^+$ T cells were not completely depleted in all the tissues examined, except in the small intestine. These results suggest that the small intestine is the tissue most sensitive to virus-induced $CD4^+$ T-cell depletion during the acute phase of infection. Recent reports revealed that severe acute depletions

FIG. 3. Profiles of $CD4^+$ T cells in systemic lymphoid tissues during acute infection. (A) Immunohistochemical staining for CD4 molecules (stained brown) in the thymus, mesenteric (mes.) LN, and jejunum tissues of KS661- or #64-infected monkeys at 27 dpi, in addition to those of uninfected monkeys. Black scale bars, 100 μm; white scale bars in insets of panels g, h, and i, 50 μm. (B) Comparison of $CD4^+$ cell frequencies in the jejunum LPL of uninfected and #64-infected monkeys at 27 dpi. A total of forty randomly selected fields (total magnification, ×400) of at least four tissue sections per animal were used for the analysis of jejunum LPL. *P* values (determined by Student's *t* test with 95% confidence intervals) are for comparisons of each #64-infected monkey with uninfected monkeys. (C) Percentages of $CD4^+$ T cells among total lymphocytes from KS661- and #64-infected monkeys. In each graph, data for 0 dpi (time points postinfection are shown along the *x* axis) are averages of percentages for seven uninfected control monkeys. Percentages of $CD4^+$ T cells (including CD4 and CD8 doubly positive cells) were obtained by first gating lymphocytes and then $CD3^+$ T cells with a flow cytometer. PBMC, peripheral blood mononuclear cells; Ing., inguinal; Jej., jejunum; iEL, intraepithelial lymphocytes; BM, bone marrow; Col., colon; *, $P < 0.05$ (percentage at 0 dpi versus that at 27 dpi; Student's *t* test with a 95% confidence interval).

of mucosal CD4$^+$ T cells have been observed in simian immunodeficiency virus-infected monkeys (11, 12, 24, 25) and human immunodeficiency virus-infected humans (2, 5, 13). The acute depletion of mucosal CD4$^+$ T cells and the disease outcome are correlated (1, 3, 21, 26). However, a decrease of mucosal CD4$^+$ T cells has also been observed in the early phases of natural host infections, such as SIVagm infection in African green monkeys and SIVsmm infection in sooty mangabeys, which typically do not progress to AIDS (4, 14, 19). In addition, the levels of apoptosis and immune activation and the degrees of CD4$^+$ T-cell restoration differ between progressors and nonprogressors in simian immunodeficiency virus models (4, 14, 19). Taken together, these results raise the possibility that the severe acute depletion of mucosal CD4$^+$ T cells is not sufficient to induce AIDS. The restoration of CD4$^+$ T cells and normal immune function after the severe acute depletion may define the eventual disease outcome (20). The abilities of KS661- and #64-infected monkeys to restore the immune system may be different, because KS661, but not #64, impairs thymic T-cell differentiation (18). Currently, we are focusing on the restoration of CD4$^+$ T cells and the functional aspect of the immune cells in the small intestines of animals infected with KS661 and #64 to further clarify the determinant(s) of the disease outcome.

We are grateful to James Raymond for English editing of the manuscript and to Takahito Kazama for technical support.

This work was supported, in part, by Research on Human Immunodeficiency Virus/AIDS in Health and Labor Sciences research grants from the Ministry of Health, Labor and Welfare, Japan, a grant-in-aid for scientific research from the Ministry of Education and Science, Japan, a research grant for health sciences focusing on drug innovation for AIDS from the Japan Health Sciences Foundation, and a grant from the Program for the Promotion of Fundamental Studies in Health Sciences of the National Institute of Biomedical Innovation (NIBIO) of Japan.

REFERENCES

1. **Brenchley, J. M., D. A. Price, and D. C. Douek.** 2006. HIV disease: fallout from a mucosal catastrophe? Nat. Immunol. **7:**235–239.
2. **Brenchley, J. M., T. W. Schacker, L. E. Ruff, D. A. Price, J. H. Taylor, G. J. Beilman, P. L. Nguyen, A. Khoruts, M. Larson, A. T. Haase, and D. C. Douek.** 2004. CD4$^+$ T cell depletion during all stages of HIV disease occurs predominantly in the gastrointestinal tract. J. Exp. Med. **200:**749–759.
3. **Chase, A., Y. Zhou, and R. F. Siliciano.** 2006. HIV-1-induced depletion of CD4$^+$ T cells in the gut: mechanism and therapeutic implications. Trends Pharmacol. Sci. **27:**4–7.
4. **Gordon, S. N., N. R. Klatt, S. E. Bosinger, J. M. Brenchley, J. M. Milush, J. C. Engram, R. M. Dunham, M. Paiardini, S. Klucking, A. Danesh, E. A. Strobert, C. Apetrei, I. V. Pandrea, D. Kelvin, D. C. Douek, S. I. Staprans, D. L. Sodora, and G. Silvestri.** 2007. Severe depletion of mucosal CD4$^+$ T cells in AIDS-free simian immunodeficiency virus-infected sooty mangabeys. J. Immunol. **179:**3026–3034.
5. **Guadalupe, M., E. Reay, S. Sankaran, T. Prindiville, J. Flamm, A. McNeil, and S. Dandekar.** 2003. Severe CD4$^+$ T-cell depletion in gut lymphoid tissue during primary human immunodeficiency virus type 1 infection and substantial delay in restoration following highly active antiretroviral therapy. J. Virol. **77:**11708–11717.
6. **Igarashi, T., C. R. Brown, R. A. Byrum, Y. Nishimura, Y. Endo, R. J. Plishka, C. Buckler, A. Buckler-White, G. Miller, V. M. Hirsch, and M. A. Martin.** 2002. Rapid and irreversible CD4$^+$ T-cell depletion induced by the highly pathogenic simian/human immunodeficiency virus SHIV(DH12R) is systemic and synchronous. J. Virol. **76:**379–391.
7. **Igarashi, T., Y. Endo, G. Englund, R. Sadjadpour, T. Matano, C. Buckler, A. Buckler-White, R. Plishka, T. Theodore, R. Shibata, and M. A. Martin.** 1999. Emergence of a highly pathogenic simian/human immunodeficiency virus in a rhesus macaque treated with anti-CD8 mAb during a primary infection with a nonpathogenic virus. Proc. Natl. Acad. Sci. USA **96:**14049–14054.
8. **Joag, S. V., Z. Li, L. Foresman, E. B. Stephens, L.-J. Zhao, I. Adany, D. M. Pinson, H. M. McClure, and O. Narayan.** 1996. Chimeric simian/human immunodeficiency virus that causes progressive loss of CD4$^+$ T cells and AIDS in pig-tailed macaques. J. Virol. **70:**3189–3197.
9. **Kato, S., Y. Hiraishi, N. Nishimura, T. Sugita, M. Tomihama, and T. Takano.** 1998. A plaque hybridization assay for quantifying and cloning infectious human immunodeficiency virus type 1 virions. J. Virol. Methods **72:**1–7.
10. **Kozyrev, I. L., K. Ibuki, T. Shimada, T. Kuwata, T. Takemura, M. Hayami, and T. Miura.** 2001. Characterization of less pathogenic infectious molecular clones derived from acute-pathogenic SHIV-89.6p stock virus. Virology **282:**6–13.
11. **Li, Q., L. Duan, J. D. Estes, Z. M. Ma, T. Rourke, Y. Wang, C. Reilly, J. Carlis, C. J. Miller, and A. T. Haase.** 2005. Peak SIV replication in resting memory CD4$^+$ T cells depletes gut lamina propria CD4$^+$ T cells. Nature **434:**1148–1152.
12. **Mattapallil, J. J., D. C. Douek, B. Hill, Y. Nishimura, M. Martin, and M. Roederer.** 2005. Massive infection and loss of memory CD4$^+$ T cells in multiple tissues during acute SIV infection. Nature **434:**1093–1097.
13. **Mehandru, S., M. A. Poles, K. Tenner-Racz, A. Horowitz, A. Hurley, C. Hogan, D. Boden, P. Racz, and M. Markowitz.** 2004. Primary HIV-1 infection is associated with preferential depletion of CD4$^+$ T lymphocytes from effector sites in the gastrointestinal tract. J. Exp. Med. **200:**761–770.
14. **Milush, J. M., J. D. Reeves, S. N. Gordon, D. Zhou, A. Muthukumar, D. A. Kosub, E. Chacko, L. D. Giavedoni, C. C. Ibegbu, K. S. Cole, J. L. Miamidian, M. Paiardini, A. P. Barry, S. I. Staprans, G. Silvestri, and D. L. Sodora.** 2007. Virally induced CD4$^+$ T cell depletion is not sufficient to induce AIDS in a natural host. J. Immunol. **179:**3047–3056.
15. **Miyake, A., Y. Enose, S. Ohkura, H. Suzuki, T. Kuwata, T. Shimada, S. Kato, O. Narayan, and M. Hayami.** 2004. The quantity and diversity of infectious viruses in various tissues of SHIV-infected monkeys at the early and AIDS stages. Arch. Virol. **149:**943–955.
16. **Miyake, A., K. Ibuki, Y. Enose, H. Suzuki, R. Horiuchi, M. Motohara, N. Saito, T. Nakasone, M. Honda, T. Watanabe, T. Miura, and M. Hayami.** 2006. Rapid dissemination of a pathogenic simian/human immunodeficiency virus to systemic organs and active replication in lymphoid tissues following intrarectal infection. J. Gen. Virol. **87:**1311–1320.
17. **Miyake, A., K. Ibuki, H. Suzuki, R. Horiuchi, N. Saito, M. Motohara, M. Hayami, and T. Miura.** 2005. Early virological events in various tissues of newborn monkeys after intrarectal infection with pathogenic simian human immunodeficiency virus. J. Med. Primatol. **34:**294–302.
18. **Motohara, M., K. Ibuki, A. Miyake, Y. Fukazawa, K. Inaba, H. Suzuki, K. Masuda, N. Minato, H. Kawamoto, T. Nakasone, M. Honda, M. Hayami, and T. Miura.** 2006. Impaired T-cell differentiation in the thymus at the early stages of acute pathogenic chimeric simian-human immunodeficiency virus (SHIV) infection in contrast to less pathogenic SHIV infection. Microbes Infect. **8:**1539–1549.
19. **Pandrea, I. V., R. Gautam, R. M. Ribeiro, J. M. Brenchley, I. F. Butler, M. Pattison, T. Rasmussen, P. A. Marx, G. Silvestri, A. A. Lackner, A. S. Perelson, D. C. Douek, R. S. Veazey, and C. Apetrei.** 2007. Acute loss of intestinal CD4$^+$ T cells is not predictive of simian immunodeficiency virus virulence. J. Immunol. **179:**3035–3046.
20. **Picker, L. J.** 2006. Immunopathogenesis of AIDS virus infection. Curr. Opin. Immunol. **18:**399–405.
21. **Picker, L. J., and D. I. Watkins.** 2005. HIV pathogenesis: the first cut is the deepest. Nat. Immunol. **6:**430–432.
22. **Reimann, K. A., J. T. Li, R. Veazey, M. Halloran, I. W. Park, G. B. Karlsson, J. Sodroski, and N. L. Letvin.** 1996. A chimeric simian/human immunodeficiency virus expressing a primary patient human immunodeficiency virus type 1 isolate *env* causes an AIDS-like disease after in vivo passage in rhesus monkeys. J. Virol. **70:**6922–6928.
23. **Shinohara, K., K. Sakai, S. Ando, Y. Ami, N. Yoshino, E. Takahashi, K. Someya, Y. Suzaki, T. Nakasone, Y. Sasaki, M. Kaizu, Y. Lu, and M. Honda.** 1999. A highly pathogenic simian/human immunodeficiency virus with genetic changes in cynomolgus monkey. J. Gen. Virol. **80:**1231–1240.
24. **Smit-McBride, Z., J. J. Mattapallil, M. McChesney, D. Ferrick, and S. Dandekar.** 1998. Gastrointestinal T lymphocytes retain high potential for cytokine responses but have severe CD4$^+$ T-cell depletion at all stages of simian immunodeficiency virus infection compared to peripheral lymphocytes. J. Virol. **72:**6646–6656.
25. **Veazey, R. S., M. DeMaria, L. V. Chalifoux, D. E. Shvetz, D. R. Pauley, H. L. Knight, M. Rosenzweig, R. P. Johnson, R. C. Desrosiers, and A. A. Lackner.** 1998. Gastrointestinal tract as a major site of CD4$^+$ T cell depletion and viral replication in SIV infection. Science **280:**427–431.
26. **Veazey, R. S., and A. A. Lackner.** 2004. Getting to the guts of HIV pathogenesis. J. Exp. Med. **200:**697–700.

Available online at www.sciencedirect.com
ScienceDirect
Antiviral Research 75 (2007) 152–158
Antiviral Research
www.elsevier.com/locate/antiviral

Suppression of virus replication via down-modulation of mitochondrial short chain enoyl-CoA hydratase in human glioblastoma cells

Megumi Takahashi [a], Eiji Watari [a], Eiji Shinya [a], Takako Shimizu [b], Hidemi Takahashi [a,*]

[a] *Department of Microbiology and Immunology, Nippon Medical School, 1-1-5 Sendagi, Bunkyo-ku, Tokyo 113-8602, Japan*
[b] *Department of Environmental Medicine, Nippon Medical School, 1-1-5 Sendagi, Bunkyo-ku, Tokyo 113-8602, Japan*

Received 17 August 2006; received in revised form 17 February 2007; accepted 21 February 2007

Abstract

Several viruses have been demonstrated to be the etiologic agent in chronic progressive diseases, associated with persistence; however, major questions concerning the pathogenic mechanisms of viral persistence are still unanswered. With the aim of identifying host cellular proteins that may play a role in viral replication, we established long-term persistently infected human glioblastoma cell lines with mutant measles virus (MV) and analyzed the host proteins by two-dimensional gel electrophoresis (2-DE) with mass spectrometry. We observed significant down-modulation in the expression of mitochondrial short chain enoyl-CoA hydratase (ECHS), which catalyzes the β-oxidation pathway of fatty acid. Knockdown of this gene by a short interference RNA (siRNA) apparently impaired wild-type MV replication and the cytopathic effects (CPEs) of MV were significantly reduced in siRNA-transfected cells. These findings will shed light upon a new important notion for the interaction between virus replication and lipid metabolism in host cells and might provide a new strategy for virus control.

Keywords: Measles virus; Persistent infection; Mitochondrial short chain enoyl-CoA hydratase; β-Oxidation; Short interference RNA

1. Introduction

A persistent viral infection is one in which a virus in a replicating or non-replicating form persists in the host beyond the normal recovery and elimination period for that particular viral infection. Although the dynamics of immune responses after acute viral infection are well studied and very consistent, the patterns of responses noted during persistent infection are more complex and differ depending on the infection. Two essential ingredients have been identified in the current understanding of persistent virus infection. The first is an immune response that is ineffectual in recognizing and clearing a virus and/or virus-infected cells; the second is that viruses can regulate the expression of both their own genes and host genes to achieve residence in a non-lytic state within the cells they infect. However, knowledge of how viral genes and cellular factors interact to cause persistence is incomplete in most instances.

In our laboratory, we have established several monkey kidney cell lines persistently infected with temperature-sensitive mutants of measles virus (MV) (Watari et al., 1979, 2001). Many aspects of these cells such as interferon production have been investigated but fail to provide a coherent mechanistic explanation for viral persistence. In this study we established a human glioblastoma cell line persistently infected with mutant measles virus, because MV persistently infect and replicate in human cells of neuronal origin and elicit subacute sclerosing panencephalitis (SSPE) in humans (Horta-Barbosa et al., 1969; Payne et al., 1969). We analyzed these persistently infected cells using two-dimensional gel electrophoresis (2-DE) in combination with tandem mass spectrometry (MS/MS), which allows us to study the alterations of host proteins during virus adaptation to the cells.

Here, we found that the expression level of mitochondrial short chain enoyl-CoA hydratase (ECHS), which catalyzes the β-oxidation pathway of fatty acid, was specifically down-modulated in persistently infected cells. Moreover, knockdown of the gene by short interference RNA (siRNA) apparently impaired wild-type MV replication, and cytopathic effects (CPEs) by MV infection were significantly reduced in siRNA-transfected cells. If one of the hallmarks of persistent infection is stable and low-level virus replication, our findings suggest that some host cellular proteins associated with lipid metabolism

* Corresponding author. Tel.: +81 3 3822 2131x5381; fax: +81 3 3316 1904.
E-mail address: htkuhkai@nms.ac.jp (H. Takahashi).

0166-3542/$ – see front matter © 2007 Elsevier B.V. All rights reserved.
doi:10.1016/j.antiviral.2007.02.002

might contribute to the regulation of virus replication followed by the establishment of persistent infection.

2. Materials and methods

2.1. Cell culture and viruses

Human glioblastoma cells, A172 and U373MG (Bender et al., 1992), were gifts from Dr. Hiroshi Takahashi (Department of Neurosurgery, Nippon Medical School, Tokyo, Japan) and were grown in Eagle's minimum essential medium (MEM, Nikken BioMedical Laboratory, Tokyo, Japan) supplemented with 10% heat-inactivated fetal calf serum, 100 U/ml of penicillin and 100 μg/ml of streptomycin. As described recently (Watari et al., 2005), wild-type Edmonston strain measles virus (Rapp clone 5) was grown and titrated on Vero cells. A temperature-sensitive mutant virus P-448 was established from Rapp clone 5 described previously (Yamaji et al., 1975). To establish persistently infected cells, A172 cells grown as monolayers were infected with P-448 mutant virus at a multiplicity of 0.1. Infected cells were passaged for the first time at 24 days' post-infection. Since the first passage, cells have been passaged weekly and were termed 448-A172 cells. For virus titration, serial tenfold dilutions of cell supernatants and cell lysates were inoculated into each of four wells of Vero cells and then incubated for 5 days. After incubation, wells were scored for CPE and we determined the dilution as $TCID_{50}$/ml at which 50% of the wells were infected.

2.2. Cell staining

For morphological analysis, cells grown on the culture plate were washed with PBS and fixed in 4% paraformaldehyde or acetone for 10 min, then cells were stained with hematoxylin solution. For immunochemical analysis, a cytospin preparation of A172 cells infected with wild-type MV and 448-A172 cells was incubated with vaccinated human serum with MV. After washing, they were overlaid with fluorescein isothiocyanate-conjugated goat anti-human antibody (Tago, Inc., Burlingame, CA).

2.3. Preparation of protein samples

The cell pellet (5×10^6 cells/sample) was disrupted in sample re-hydration buffer (8 M urea, 2% CHAPS, 0.5% ZOOM Carrier Ampholytes, 20 mM dithiothreitol (DTT), 0.002% bromophenol blue; Invitrogen, Carlsbad, CA) at room temperature for 15 min. The lysate was separated by centrifugation at $10{,}000 \times g$ for 5 min to yield supernatant that was stored at −80 °C until use. To visualize low-abundance proteins more efficiently, we prepared sub-cellular fraction of cells using a proteome extraction kit (Calbiochem, Darmstadt, Germany).

2.4. Two-dimensional gel electrophoresis

Cell lysate in re-hydration buffer was applied to ZOOM strips (pH 4–7, Invitrogen) in a total volume of 155 μl. After re-hydration for 16 h at room temperature, proteins were separated by isoelectrofocusing (IEF) at room temperature and 50 mA/strip with the following linear voltage increases: 200 V for 20 min, 450 V for 15 min, 750 V for 15 min, and 2000 V for 30 min. The strips were equilibrated in 50 mM Tris containing 6 M urea, 30% glycerol, 2% sodium dodecylsulfate (SDS) and 2% DTT for 20 min. The second dimension was performed on 13% SDS-polyacrylamide gels. Separated protein spots were fixed and stained on the gel with a silver staining kit (Nacalai Tesque, Kyoto, Japan). Differential spots were excised from silver-stained gels and treated with 20 μg of trypsin/ml in 50 mM ammonium bicarbonate buffer at 37 °C overnight. After in-gel digestion, the digested solution was transferred into a clean tube and dried under vacuum. The resulting samples were dissolved in 20 μl of 2% acetonitrile and 0.1% trifluoroacetic acid, and applied to LC–MS/MS analysis.

2.5. Identification of protein spots

Analysis was performed using an LC–MS/MS system with RP-mLC composed of a Paradigm MS4 dual solvent delivery system (Michrom BioResources, Auburn, CA), a HTC PAL auto sampler with two 10-port injector valves (CTC Analytics), Finnigan LCQ Deca XP plus (Thermo Electron, Waltham, MA) equipped with NSI sources (AMR Inc., Tokyo, Japan). The mass spectrometer was operated in data-dependent acquisition mode in which MS acquisition with a mass range of m/z 450–2000 was automatically switched to MS/MS acquisition under the automated control of Xcalibur software. The capillary exit of the electrospray ion source was set at 70 V, the octapole at 3 V, and the capillary temperature at 250 °C. A counter flow of helium was used as nebulizing gas. Each sample was injected onto a capillary RP column, MAGIC C18 (3 mm, 200 Å, 50 m × 0.2 m i.d., Michrom BioResources) with an acetonitrile linear gradient of 3 ml/min in formic acid 0.1%, from 2 to 60%. The HPLC column was rinsed with 90% acetonitrile in 0.1% formic acid between each injection.

2.6. siRNA transfection

A172 cells were plated in 48-well tissue culture plates at 1×10^5 cells/well in 150 μl MEM on the day of transfection. Cells were transfected with 1 μl HiPerFect Transfection Reagent (Qiagen, Düsseldorf, Germany) and 1 μl siRNAs (5 nM) in a total volume of 100 μl DMEM (Sigma–Aldrich, St. Louis, MO) according to the manufacturer's protocol. At 48 h after transfection, cells were infected with viruses and their growth on transfected cells was analyzed using the $TCID_{50}$ protocol. The siRNA oligonucleotides targeted the ECHS gene at position 864–884 (termed #864: aaagagaaaggccaacttcaa), 865–885 (termed #865: aagagaaaggccaacttcaaa), 1088–1108 (termed #1088: ctggcgcgccttctaaatcta), and 1245–1265 (termed #1245: cagatgctgattaaagtgata). These siRNAs were synthesized by Qiagen. Non-silencing siRNA with no known homology to mammalian genes was a commercially available duplex (Qiagen) and was used as control siRNA.

2.7. Quantitative RT-PCR

RNA was prepared from siRNA-transfected A172 cells using RNAeasy (Qiagen). One microgram of RNA was incubated for 1 h at 42 °C after adding 20 U of RNase inhibitors (TaKaRa, Bio Inc., Otsu, Japan), 0.2 mM deoxynucleoside triphosphates, 2.5 nM random primers, 11 U of Rous associated virus 2 reverse transcriptase (TaKaRa) and reverse transcriptase buffer to a final volume of 20 μl. One microlitre of RT reaction mixture was used as a template for real-time PCR using SYBR Green PCR Master Mix (Applied Biosystems, Foster City, CA) with the following primers specific for ECHS (forward, cgctgctgtcaatggctatg, and reverse, cttggcgtcctgggctgaga), β-actin (forward, tcacccacactgcccatctacga, and reverse, cagcggaaccgctcattgccaatgg), MV-NP protein (forward, tcagtagagcggttggaccc, and reverse, ggcccggtttctctgtagct), MV-H protein (forward, ttcatcgggcagccatctac, and reverse, ctctgaggtgtcctcaggcc), MV-F protein (forward, gcgagcctggaaactactaatca, and reverse, ccctgaacagccaatatcatctc). The amount of each ECHS mRNA was normalized to that of β-actin mRNA in the same sample.

2.8. Measurement of cell growth

Single cell suspensions were seeded at a density of 5×10^4 cells/well on 96-well microtiter plates. After 1–3 days of incubation, the cells were pulse-labeled with 0.5 μCi methyl-^{3}H-thymidine/well for the last 8 h, and were then harvested and counted using a β-counter (1450 Microbeta Trilux; Wallac, Gaithersburg, MD).

2.9. Western blotting

A172 cells treated with or without siRNA were infected with MV. After 2 days' infection, cells were lysed in 30 μl of lysis buffer (1% Nonidet P-40, 140 mM NaCl, 20 mM Tris–HCl (pH 8.0), 2 mM EDTA, 1 mM sodium orthovanadate, 1 mM PMSF, and 50 mM monoiodoacetamide) on ice for 15 min. After centrifugation at 20,400 × *g* for 15 min, proteins in cell lysates were separated by 10% SDS-PAGE under reducing conditions and transferred to a nylon membrane. The blots were probed with vaccinated human serum with MV or mouse anti-β-actin (clone AC-74, Sigma, St. Louis, MO) followed by peroxidase-

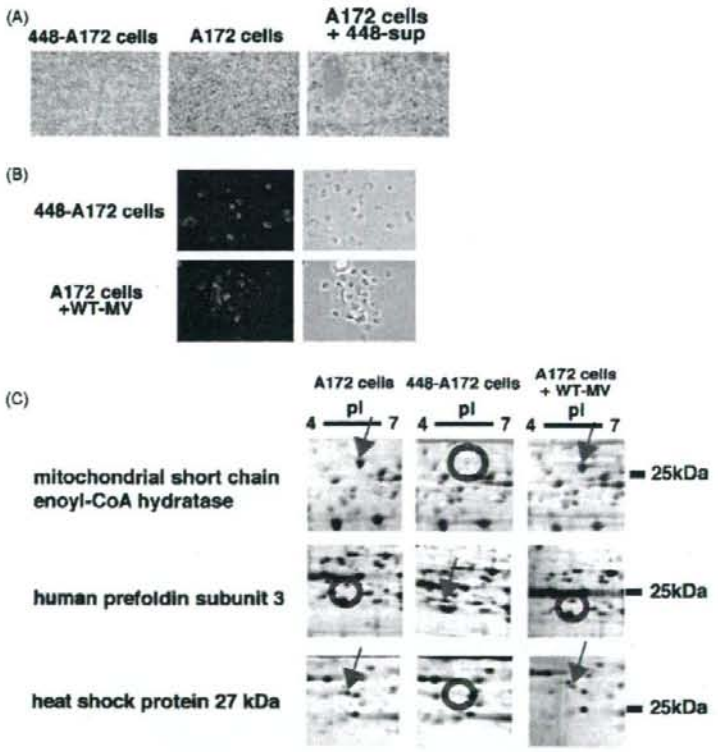

Fig. 1. Characterization of 448-A172 cells persistently infected mutant MV. (A) Morphology of 448-A172 cells (left), A172 cells (middle), and A172 cells treated with supernatants from 448-A172 cells. Cells were stained with hematoxylin solution. (B) Detection of virus antigens with vaccinated human serum with MV in 448-A172 cells (upper) or A172 cells infected with wild-type MV (lower). (C) Silver-stained two-dimensional gels of A172 cells (left column), 448-A172 cells (middle column), or A172 cells infected with wild-type MV (right column). Mitochondrial short-chain enoyl-CoA hydratase (ECHS) was detected in whole cell fraction, human prefoldin subunit 3 was detected in cytosolic fraction, and heat shock protein 27 kDa was detected in nucleus fraction.

conjugated rabbit anti-human IgG (MP Biomedicals, Irvine, CA) or goat anti-mouse IgG (Jackson ImmunoResearch, West Grove, PA). Bands were visualized using a tetramethylbenzidine substrate kit (Vector, Burlingame, CA).

3. Results

3.1. Establishment and analysis of a cell line persistently infected with temperature-sensitive mutant measles virus

To investigate the mechanisms underlying virus persistence, we established a human glioblastoma cell line persistently infected with a temperature-sensitive mutant MV named 448-A172 after about 50 days of infection. The appearance of the 448-A172 cell line was indistinguishable from intact uninfected A172 cells (Fig. 1A). Thus, the situation of persistent MV infection in 448-A172 cells was examined by the detection of intracellular viral antigens using an immunofluorescent technique. As shown in Fig. 1B, viral antigens were mainly observed in the cytoplasms of 448-A172 cells, and infectious virions from cells could be obtained and titrated on Vero cell monolayers. Indeed, culture supernatants harvested on day 4 contained measurable amounts of viruses (10^4 $TCID_{50}$/ml) that induced syncytial cell formation for intact A172 cells (Fig. 1A).

3.2. Identification of proteins crucial for persistent infection in the established 448-A172 cell line

These findings suggest that such persistent infection did not depend on the type of virion but rather on host cellular conditions; therefore, to explore the possible mechanisms involved in persistent infection, we precisely compared the cellular proteins between 448-A172 cells and A172 cells infected with or without wild-type MV using 2-DE with p*I* values in the range of 4–7 to obtain a greater resolution in protein separation. The 2-DE image of cellular proteins after silver staining is shown in Fig. 1C. For the assessment of differentially expressed proteins, protein spots clearly altered in 448-A172 cells were considered. We did find three altered proteins, which were then characterized by mass spectrometry and identified as mitochondrial short chain enoyl-CoA hydratase, human prefoldin subunit 3, and heat shock protein 27 kDa.

3.3. Inhibition of ECHS expression with specific siRNA

Among those three proteins, we focused on investigating the functional role of ECHS for viral replication, because ECHS protein is more abundant than other proteins in intact A172 cells and the amount of ECHS is obviously reduced in 448-A172 cells. Using quantitative RT-PCR analysis quantifying ECHS transcripts relative to that of β-actin from 448-A172 cells, we confirmed that the expression levels of ECHS mRNA in 448-A172 cells was decreased to less than 10% in comparison with intact A172 cells (data not shown). Then, ECHS-specific siRNAs were prepared to evaluate the potential involvement of ECHS in regulating the replication of MV. Four different siRNAs were used to specifically knockdown the expression of ECHS in intact

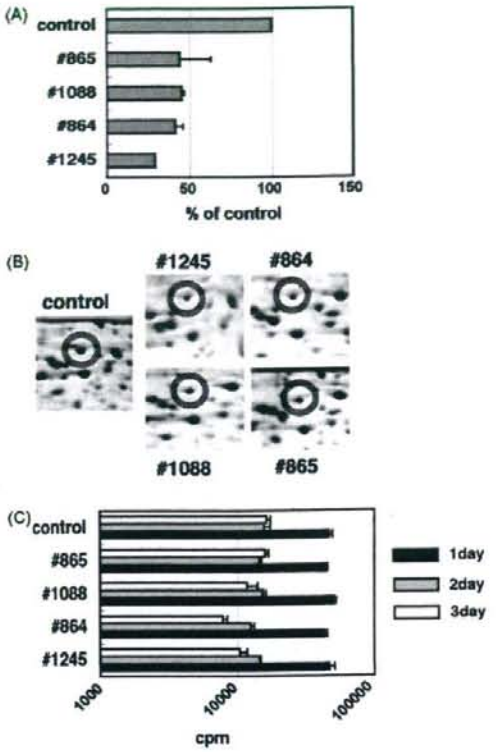

Fig. 2. Effect of siRNA transfection on A172 cells. (A) A172 cells were transfected with each siRNA. Total RNA was isolated from cells 24 h after transfection and was subjected to quantitative RT-PCR specific for ECHS or β-actin primer. Data were normalized to the amount of β-actin mRNA and are expressed as percentages of the normalized value for control siRNA-transfected cells. Values are the mean ± standard deviation (S.D.) of at least three experiments. (B) A172 cells were transfected with each siRNA. After 48 h incubation, cells were lysed and subjected to 2-DE analysis. Gels were visualized with silver staining. (C) A172 cells were transfected with each siRNA. After 1–3 days' incubation, the cells were pulse-labeled with 0.5 μCi/well methyl-^{3}H-thymidine for the last 8 h.

A172 cells. Twenty-four or 48 h post-transfection with a siRNA, mRNA and protein levels of ECHS in A172 cells were reduced up to 30–45% of control siRNA-transfected cells (Fig. 2A and B). As ECHS catalyzes the second step in the β-oxidation pathway of fatty acid metabolism, down-modulation of ECHS might result in the deficient production of energy-yielding substrates via β-oxidation. Therefore, we examined the effect of ECHS suppression on cell proliferation using the ^{3}H-thymidine uptake method. Although siRNA had little effect on cell proliferation until 2 days after transfection, the reduction of ^{3}H-thymidine uptake was observed in three siRNA-transfected cells, but no dead cells were detected 3 days after transfection (Fig. 2C).

3.4. Inhibition of MV replication by ECHS siRNA in A172 cells

To see whether the treatment of cells with ECHS-specific siRNA can inhibit MV replication, we examined their inhibitory

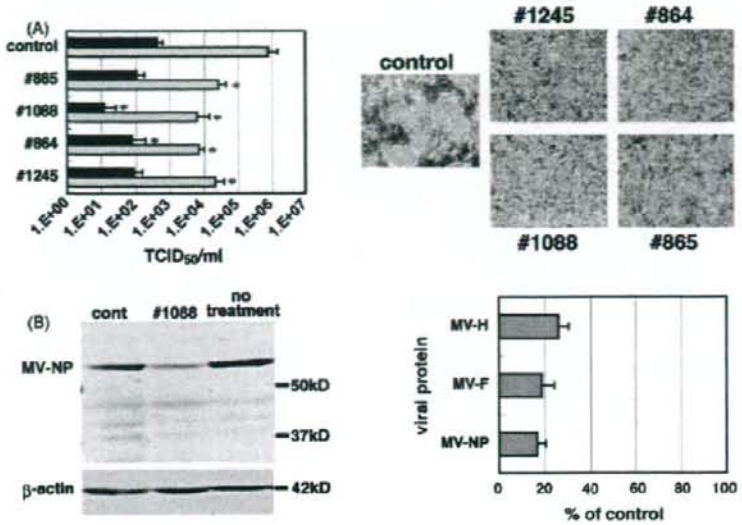

Fig. 3. Effect of siRNA transfection on MV replication. (A) A172 cells were transfected with each siRNA. After 48 h incubation, A172 cells were infected with wild-type MV, and then both cells (gray bars) and supernatants (charcoal bars) were harvested at 48 h after infection followed by determination of the virus titer (left). Data are expressed as the virus titer ($TCID_{50}$) and are the means ± S.D. of values of at least three independent experiments. $^{*}P < 0.05$ vs. the value of cells transfected with control siRNA (Student's *t*-test). Cells were stained with hematoxylin solution after 48 h infection (right). (B, left) A172 cells treated with or without siRNA were infected with MV. After 2 days' infection, cells were lysed in 30 μl of lysis buffer, and proteins in lysates were separated in 10% polyacrylaminde gel and blotted on a nylon membrane. The blot was probed with vaccinated human serum with MV (upper column) or mouse anti-β-actin antibody (lower column). (B, right) A172 cells treated with or without siRNA were infected with MV. After 2 days' infection, total RNA was isolated from cells 24 h after transfection and subjected to quantitative RT-PCR specific for MV-NP protein, MV-F protein or MV-H protein primer. Data were normalized to the amount of β-actin mRNA and are expressed as percentages of the normalized value for control siRNA-transfected cells. Values are the mean ± S.D. of at least three experiments.

effect on intact A172 cells. Forty-eight hours post-transfection with siRNA, A172 cells were infected with wild-type MV at a multiplicity of infection (moi) of 0.1. At 48 h after infection, culture supernatants and cells were harvested, serially diluted, and the virus titer determined (expressed as $TCID_{50}$/ml). As shown in Fig. 3A, we observed the efficient inhibition of MV replication after transfection with four distinct siRNAs. Indeed, when #1088 siRNA was used, inhibition was so pronounced that culture supernatants contained only a few viruses. CPE by MV infection observed at 48 h post-infection in control and ECHS siRNA-transfected groups is also shown in Fig. 3A. There is an apparent marked reduction of CPE in all siRNA-transfected cells. This was confirmed by titrating the virions yielded between control and siRNA-transfected cells. Moreover, Western blot analysis showed that transfection of A172 cells with #1088 siRNA reduced the accumulation of viral protein compared to cells transfected with control siRNA or without siRNA. This protein reduction was due to a decrease in the expression of viral mRNA (Fig. 3B).

3.5. *Effect of ECHS siRNA on other virus replication*

Next, to determine if ECHS is also involved in the replication of other RNA viruses, siRNA-transfected A172 cells were infected with vesicular stomatitis virus (VSV) or semliki forest virus (SFV). As demonstrated in Fig. 4A, targeting ECHS mRNA also significantly inhibited both VSV and SFV replication in A172 cells. Similar to MV infection, CPEs were not detected in all siRNA-transfected A172 cells at 24 h after VSV or SFV infection (data not shown).

ECHS catalyzes the β-oxidation pathway of fatty acid. To further analyze the involvement of β-oxidation in virus replication, we examined the effect of etomoxir (Sigma), an inhibitor of carnitine palmitoyltransferase that inhibits mitochondrial β-oxidation, on MV replication in A172 cells. Treatment of A172 cells with etomoxir resulted in the suppression of MV replication in a dose-dependent manner (Fig. 4B). These results suggest that β-oxidation might be involved in MV replication.

We also observed that treatment of A172 cells with IFN-β (1000 IU/ml) effectively inhibited MV replication by approximately 100 times (Fig. 4B), indicating that down-modulation of ECHS potency with siRNA corresponds to treatment with a high titer of IFN-β to inhibit virus replication. Recently, it was reported that siRNA treatment could nonspecifically induce IFN-mediated innate immune responses (Sledz and Williams, 2004); however, it was unlikely that IFN mediated protection in our experiments, because a large amount of IFN-α was originally produced in intact A172 cells but IFN-β was not detected in culture supernatants from intact or siRNA-transfected A172 cells (data not shown).

To extend the results in A172 cells, we further tested the ability of siRNAs to inhibit virus replication in other glioblastoma cells, U373MG. When U373MG cells were transfected with each siRNA and then infected with MV at a moi of 0.1

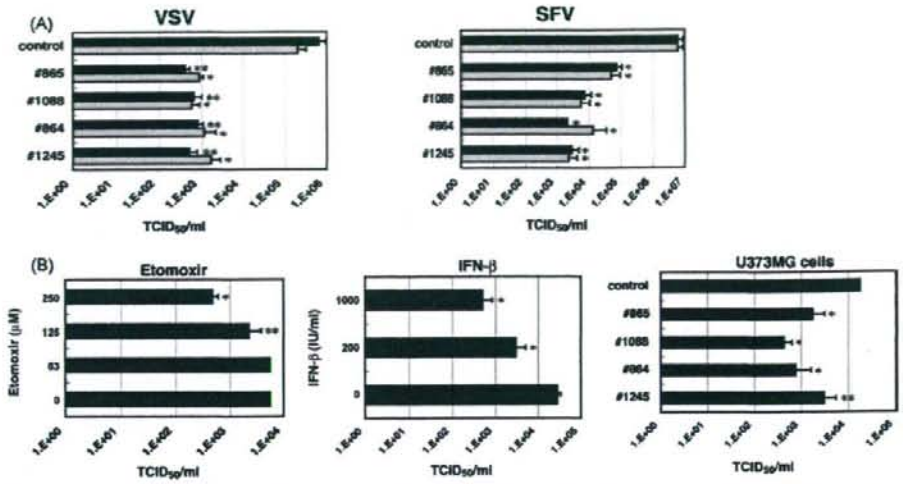

Fig. 4. Effect of siRNA transfection on other virus replication. (A) A172 cells were transfected with each siRNA. After 48 h incubation, A172 cells were infected with VSV (left) or SFV (right) at a moi of 0.1, and then cells (gray bars) and supernatants (charcoal bars) were harvested at 24 h after infection followed by determination of the virus titer. (B) A172 cells were treated with the indicated concentration of etomoxir (left). After 48 h incubation, A172 cells were infected with wild-type MV, and then supernatants were harvested at 72 h after infection followed by the assay for determination of the virus titer. A172 cells were treated with the indicated concentration of IFN-β (middle). After 24 h incubation, cells were infected with wild-type MV, and then supernatants were harvested at 48 h after infection followed by determination of the virus titer. U373MG cells were transfected with each siRNA (right). After 48 h incubation, U373MG cells were infected with wild-type MV, and then supernatants were harvested at 48 h after infection followed by determination of the virus titer. Data are expressed as the virus titer ($TCID_{50}$) and are the means ± standard deviations (S.D.) of values of at least three independent experiments. (A and B) $^{*}P<0.02$, and $^{**}P<0.05$ vs. the value of cells transfected with control siRNA or treated without reagents.

at 48 h post-transfection, siRNA, especially #864 and #1088, significantly inhibited virus replication (Fig. 4B). Moreover, to confirm whether stable infection with mutant MV in other cells induce the down-modulation of ECHS expression as well as 448-A172 cells, we are now attempting to establish a cell line persistently infected with mutant MV using U373MG cells.

4. Discussion

In this study, we have found that the expression of ECHS protein was significantly down-modulated in cells persistently infected with temperature-sensitive mutant MV. Moreover, similar to conventional MV, the mutant MV produced and secreted from persistently infected cells showed the capacity to induce syncytial formation upon infection to normal A172 human glioblastoma cells, indicating that such persistent infection is not due to the type of virion but rather to host cellular conditions. We thus speculate the ECHS gene as an essential host cellular gene utilized for virus replication, and conducted experiments to inhibit host cellular ECHS with siRNA by the gene-transfer technique. As expected, the replication of wild-type MV was specifically blocked by siRNA via knockdown of the ECHS gene.

ECHS catalyzes the second step in the physiologically important β-oxidation pathway of fatty acid metabolism (Agnihotri and Liu, 2003). In mammals, fatty acid oxidation occurs in mitochondria, peroxisomes, and smooth endoplasmic reticulum. Although mitochondria and peroxisomes oxidize fatty acids via β-oxidation, smooth endoplasmic reticulum metabolizes fatty acids by ω-oxidation. Such mitochondrial β-oxidation is responsible for oxidation in the major portion of short- (<C8), medium- (C8-12), and long- (C14-20) chain fatty acids and, in that process, constitutes the primary source of energy derived from fatty acids. The catalytic mechanism of ECHS has been studied in great depth through a combination of kinetic, spectroscopic, and structural techniques (Kim and Battaile, 2002); however, the expression and gene regulation of this enzyme have not been fully elucidated. Several reports have shown that the expression level of ECHS was decreased in cancer cell lines and carcinoma (Balabanov et al., 2001; Fratelli et al., 2003; Hwa et al., 2005; Sakata et al., 1998). Although the biological significance of ECHS in human cancer has not been confirmed, regulation of this enzyme by a carcinogen might have a role in the proliferation and differentiation of normal cells. On the other hand, very few reports refer to the interaction between ECHS and microbial infections. Only Yokoyama et al. have reported that the expression level of ECHS was decreased in hepatocellular carcinoma from patients infected with hepatitis C virus (Yokoyama et al., 2004).

Although we have not yet elucidated the molecular mechanism for the regulation of MV replication by ECHS, down-modulation of ECHS inevitably leads to the inhibition of β-oxidation. We also found that treatment of A172 cells with etomoxir, an inhibitor of β-oxidation, effectively suppressed virus replication. These findings suggest that β-oxidation appeared to be involved in MV replication; moreover, the fact that ECHS

siRNA also effectively interfered with VSV or SFV replication in A172 cells indicates that β-oxidation might be essential for the common replication cycles of various viruses.

Recently, there have been significant advances in identifying cellular factors that promote or inhibit viral replication. In the case of HIV-1, novel factors such as APOBEC or TRIM5α have been discovered (Sheehy et al., 2002; Stremlau et al., 2004). Both proteins show anti-viral activity; in particular, APOBEC family proteins have activity in a wide variety of viruses. Consequently, up-modulation of these proteins in host cells imparts resistance to viral replication. Taken together, there may be two concepts for suppressing virus replication in host cells: the lack of an essential factor for virus replication and the presence of an efficient mechanism for controlling replication. APOBEC proteins seem to correspond only to the latter mechanism, while ECHS might correspond to both, because the impairment of β-oxidation might result in the reduction of energy-yielding substrates (acetyl-CoA and ketone bodies), which eventually leads to a shortage of ATP, and adversely cause the accumulation of both free fatty acids and toxic acyl-CoA intermediates in cells.

Although the expression level of ECHS in 448-A172 cells seemed significantly lower than that in siRNA-transfected cells, culture supernatants from the 448-A172 cells still contained measurable amounts of viruses (10^4 $TCID_{50}$/ml) and their growth rate was almost the same as #864-siRNA-transfected cells. These data suggest that other host factors relating to viral replication besides ECHS might be stably disturbed in 448-A712 cells. Indeed, we found that human prefoldin subunit 3 and heat shock protein 27 kDa seemed to down-modulate virus replication and extend cell survival (Fig. 1C). Further investigation on another host proteins must be required to understand the precise mechanisms how viral genes and cellular factors interact to cause persistent viral infection.

One of the hallmarks of persistent infection is to create an excellent intracellular status for stable and low-level virus replication. The reduction of ECHS may contribute not only to low steady-state levels of virus replication but also to the survival of virus-infected cells. The suppression of virus replication might help to prolong the asymptomatic phase of virus infection; therefore, further precise analysis of the molecular regulation of our findings shown here might cast new light on the development of novel anti-viral drugs concerned with lipid metabolism. Indeed, Sakamoto et al. recently identified an HCV replication inhibitor which prevents the de novo synthesis of sphingolipids, a major lipid raft component (Sakamoto et al., 2005).

Acknowledgements

We thank Drs. Takahiro Isono, Noriyuki Nagahara and Masayasu Minami for experimental advice on the proteomic analysis. This work was supported in part by grants from the Ministry of Education, Science, Sport, and Culture, from the Ministry of Health and Labor and Welfare, Japan, from the Japanese Health Sciences Foundation, and from the Promotion and Mutual Aid Corporation for Private School of Japan.

Appendix A. Supplementary data

Supplementary data associated with this article can be found, in the online version, at doi:10.1016/j.antiviral.2007.02.002.

References

Agnihotri, G., Liu, H.W., 2003. Enoyl-CoA hydratase. reaction, mechanism, and inhibition. Bioorg. Med. Chem. 11, 9–20.

Balabanov, S., Zimmermann, U., Protzel, C., Scharf, C., Klebingat, K.J., Walther, R., 2001. Tumour-related enzyme alterations in the clear cell type of human renal cell carcinoma identified by two-dimensional gel electrophoresis. Eur. J. Biochem. 268, 5977–5980.

Bender, H., Takahashi, H., Adachi, K., Belser, P., Liang, S.H., Prewett, M., Schrappe, M., Sutter, A., Rodeck, U., Herlyn, D., 1992. Immunotherapy of human glioma xenografts with unlabeled, 131I-, or 125I-labeled monoclonal antibody 425 to epidermal growth factor receptor. Cancer Res. 52, 121–126.

Fratelli, M., Demol, H., Puype, M., Casagrande, S., Villa, P., Eberini, I., Vandekerckhove, J., Gianazza, E., Ghezzi, P., 2003. Identification of proteins undergoing glutathionylation in oxidatively stressed hepatocytes and hepatoma cells. Proteomics 3, 1154–1161.

Horta-Barbosa, L., Fuccillo, D.A., London, W.T., Jabbour, J.T., Zeman, W., Sever, J.L., 1969. Isolation of measles virus from brain cell cultures of two patients with subacute sclerosing panencephalitis. Proc. Soc. Exp. Biol. Med. 132, 272–277.

Hwa, J.S., Park, H.J., Jung, J.H., Kam, S.C., Park, H.C., Kim, C.W., Kang, K.R., Hyun, J.S., Chung, K.H., 2005. Identification of proteins differentially expressed in the conventional renal cell carcinoma by proteomic analysis. J. Kor. Med. Sci. 20, 450–455.

Kim, J.J., Battaile, K.P., 2002. Burning fat: the structural basis of fatty acid beta-oxidation. Curr. Opin. Struct. Biol. 12, 721–728.

Payne, F.E., Baublis, J.V., Itabashi, H.H., 1969. Isolation of measles virus from cell cultures of brain from a patient with subacute sclerosing panencephalitis. N. Engl. J. Med. 281, 585–589.

Sakamoto, H., Okamoto, K., Aoki, M., Kato, H., Katsume, A., Ohta, A., Tsukuda, T., Shimma, N., Aoki, Y., Arisawa, M., Kohara, M., Sudoh, M., 2005. Host sphingolipid biosynthesis as a target for hepatitis C virus therapy. Nat. Chem. Biol. 1, 333–337.

Sakata, M., Kurachi, H., Morishige, K., Ogura, K., Yamaguchi, M., Nishio, Y., Ikegami, H., Miyake, A., Murata, Y., 1998. Messenger RNA differential display reverse-transcriptase-polymerase-chain-reaction analysis of a progestogen-suppressive gene in a human endometrial-cancer cell line. Int. J. Cancer 78, 125–129.

Sheehy, A.M., Gaddis, N.C., Choi, J.D., Malim, M.H., 2002. Isolation of a human gene that inhibits HIV-1 infection and is suppressed by the viral Vif protein. Nature 418, 646–650.

Sledz, C.A., Williams, B.R., 2004. RNA interference and double-stranded-RNA-activated pathways. Biochem. Soc. Trans. 32, 952–956.

Stremlau, M., Owens, C.M., Perron, M.J., Kiessling, M., Autissier, P., Sodroski, J., 2004. The cytoplasmic body component TRIM5alpha restricts HIV-1 infection in Old World monkeys. Nature 427, 848–853.

Watari, E., Yamanaka, A.M., Yamaji Y, M., 1979. Establishment of persistent infection of measles virus in Vero cells with special reference to the temperature-sensitivity of parent viruses. J. Nippon Med. Sch. 46, 147–150.

Watari, E., Shimizu, M., Takahashi, H., 2005. Langerhans cells stimulated by mechanical stress are susceptible to measls virus. Intervirology 48, 145–152.

Watari, E., Shinya, E., Kurane, S., Takahashi, H., 2001. Effects of cyclosporin A on cell fusion in a monkey kidney cell line persistently infected with measles virus. Intervirology 44, 209–214.

Yamaji, Y., Honda, B.F., Todome, H., Suganuma, Y., Watari, M., Iwaguchi, E., Nagashima M, H., 1975. Characterzation of temperature-sensitive mutants of measles virus: temperature-shift experiment. Jpn. J. Med. Sci. Biol. 28, 223–229.

Yokoyama, Y., Kuramitsu, Y., Takashima, M., Iizuka, N., Toda, T., Terai, S., Sakaida, I., Oka, M., Nakamura, K., Okita, K., 2004. Proteomic profiling of proteins decreased in hepatocellular carcinoma from patients infected with hepatitis C virus. Proteomics 4, 2111–2116.

Biophysical Journal Volume 92 April 2007 2570–2582

Molecular Analysis of TCR and Peptide/MHC Interaction Using P18-I10-Derived Peptides with a Single D-Amino Acid Substitution

Yohko Nakagawa,* Hiroto Kikuchi,† and Hidemi Takahashi*
*Department of Microbiology and Immunology and †Department of Physics, Nippon Medical School, Tokyo 113-8602, Japan

ABSTRACT For the structural analysis of T-cell receptor (TCR) and peptide/MHC interaction, a series of peptides with a single amino acid substitution by a corresponding D-amino acid, having the same weight, size, and charge, within P18-I10 (aa318–327: RGPGRAFVTI), an immunodominant epitope of HIV-1 IIIB envelope glycoprotein, restricted by the H-2D^d class I MHC molecule, has been synthesized. Using those peptides, we have observed that the replacement at positions 324F, 325V, 326T, and 327I with each corresponding D-amino acid induced marked reduction of the potency to sensitize targets for P18-I10-specific murine CD8$^+$ cytotoxic T lymphocytes (CTLs), LINE-IIIB, recognition. To analyze further the role of amino acid at position 325, the most critical site for determining epitope specificity, we have developed a CTL line [LINE-IIIB(325D)] and its offspring clones specific for the epitope I-10(325v) having a D-valine (v) at position 325. Taking advantage of two distinct sets of CD8$^+$ CTLs restricted by the same D^d, three-dimensional structural analysis on TCR and peptide/MHC complexes by molecular modeling was performed, which indicates that the critical amino acids within the TCRs for interacting with 325V or 325v appear to belong to the complementarity-determining region 1 but not to the complementarity-determining region 3 of Vβ chain.

INTRODUCTION

Immune responses to viral infection include both humoral and cell-mediated effector mechanisms. The major effector cells in cellular immunity are CD8 molcule-expressing cytotoxic T lymphocytes (CTLs) that can recognize and kill virus-infected cells. In general, endogenously synthesized antigens such as virus-derived proteins are fragmented inside of the cells and are presented on the cell in conjunction with class I major histocompatibility complex (MHC) molecules. Such processed epitope peptides associated with the class I MHC molecules can be recognized by CTLs via their specific T cell receptors (TCRs).

The TCRs expressed on the cell surface of T lymphocytes contain similar structural patterns with immunoglobulin-like domains, comprising one variable and one constant, as well as a transmembrane domain and a short cytoplasmic tail. The specificity for T-cell recognition seems to be determined by the variable domains, TCR Vα and TCR Vβ, within two heterodimeric subsets, TCRα and TCRβ. Several recent findings have indicated that the TCRα and β heterodimers are oriented to the long axis of the epitope-peptide/MHC complex (1), in which the Vα domain appears to cover the amino-terminal half of the epitope peptide, whereas Vβ is located over the carboxyl-terminal portion of the epitope (2).

Among those variable Vα and Vβ domains, three hypervariable complementarity-determining regions (CDRs), termed CDR1, CDR2, and CDR3, seem to directly interact with the peptide/MHC complex. Because the degree of variability is the greatest in the CDR3 loop generally, and it is positioned more closely over the epitope peptide than other CDR1 and CDR2 loops, the antigen specificity has been considered to be associated with the CDR3 but not with CDR1 or CDR2, which were predicted to interact principally with the MHC molecules (3,4). Indeed, according to a recent report on the murine K^b class I MHC molecule-restricted epitope octapeptide (pKB1: KVITFIDL) recognized by KB5-C20 TCR (5), TCR plasticity is primarily restricted to the CDR3 loops of the Vβ domain. Nevertheless, recent crystallographic analyses on various TCR and peptide/MHC interactions have suggested the possibility of direct contact for both CDR1 and CDR3 in the TCRα and TCRβ chains with the antigenic peptide/MHC complex (5,6). Therefore, to understand more precise molecular interactions determining T-cell specificity through TCR-mediated peptide/MHC complex recognition, we took advantage of the following known materials to accomplish the analysis.

We have established CD8$^+$, H-2D^d class I MHC molecule-restricted murine CTL line, LINE-IIIB, specific for the envelope glycoprotein 160 (gp160) composed of ~900 amino acids derived from one of the most commonly used IIIB strains of human immunodeficiency virus type-1 (HIV-1), a causative agent for acquired immunodeficiency syndrome (AIDS) (7). Then, we have identified an immunodominant epitope within the gp160 as a 15-residue peptide, P18IIIB (aa315–329: RIQRGPGRAFVTIGK), for the LINE-IIIB recognition (7) as well as the minimal active 10-residue peptide, P18-I10 (aa318–327: RGPGRAFVTI) within P18IIIB (8). Moreover, although the position of P18IIIB is located in the hypervariable portion (termed V3 domain) of the viral envelope, the site has turned out to be recognized by various isolate-specific CTLs in an isolate-specific manner (9,10), and

Submitted August 16, 2006, and accepted for publication December 13, 2006.

Address reprint requests to Hidemi Takahashi, Department of Microbiology and Immunology, Nippon Medical School, 1-1-5 Sendagi, Bunkyo-ku, Tokyo 113-8602, Japan. Tel.: 81-3-3822-2131 ext. 5381; Fax: 81-3-3316-1904; E-mail: htkuhkai@nms.ac.jp.

0006-3495/07/04/2570/13 $2.00

doi: 10.1529/biophysj.106.095208

a number of distinct class I MHC molecules did present the P18IIIB to each specific CTL (11). Furthermore, the P18IIIB in the V3-domain was found to be overlapped with the major determinant sites for neutralizing antibodies against HIV-1 in an isolate-specific manner (12–14) and also to be recognized by CD4-positive helper T lymphocytes specific for HIV-1 in a class II MHC molecule-restricted manner (8,15). In addition, human CTLs did see the P18IIIB when presented by HLA A2 and A3 (16). These findings indicate that the P18IIIB appears to be a highly attractive epitope for the development of peptide-based vaccine against AIDS, and thus, it is important to study the precise interaction between the epitope P18IIIB and their specific TCRs to study the manner of T-cell-mediated immune responses.

Using a series of peptides with an alanine (A) substitution at each position, we observed that amino acids at positions 322R and position 324F were critical for D^d binding and that position 325V within P18-I10 was essential for interacting with TCRs (17). Also, C-terminus 327I appears to be critical for D^d binding to form the D^d-binding motif (8,18). In addition, we found the HIV-MN isolate-specific CTLs also saw the corresponding minimal active site, MNT10 (aa318–327: IGPGRAFYTT) in association with the same D^d molecules, and replacement of just a single residue, 325V with 325Y, within the P18-I10 or vice versa within the MNT10 was sufficient to reciprocally interchange the specificities for these two non-cross-reactive sets of CTLs (9,10). Thus, a single side chain at position 325 can play a critical role in determining the epitope specificity within both P18-I10 and MNT10 presented by the same class I MHC molecule D^d for $CD8^+$ CTL TCR recognition mediated by the CDRs.

It has been reported that the charge of the amino acid might also affect interaction between TCRs and peptide/MHC complexes (19). Indeed, when negatively charged glutamic acid (E) at position 436 within HIV-1-envelope-derived helper T-cell epitope T1 (aa428–443; KQIINMWQEVGKAMYA) (20) was substituted with either uncharged alanine (A) or size-conservative, uncharged glutamine (Q), stimulatory capacity of the substitute peptides for T1-specific T hybridomas was significantly enhanced, although charge-conservative aspartic acid (D) substitution did not show any enhancement (21). Moreover, substitution at position 6Q in the immunodominant CTL epitope for vesicular stomatitis virus (RGYVYQGL, VSV8) presented by K^d class I MHC molecules to a negatively charged residue such as 6E or 6D induced a change at position 93S of TCR CDR3α to a positively charged residue 93R or 93K (22). Therefore, particularly to reduce the influence of charges of each amino acid as well as the size and molecular weight on TCR-mediated recognition, a series of P18-I10-derived peptides with a single amino acid substitution by D-amino acid at each corresponding site have been synthesized. Using those D-amino acid–substituted peptides, we found apparent reduction of specific cytotoxic activity in the 325V-specific LINE-IIIB cells by the replacement of 325V with D-type valine at position 325, represented as I10(325v). Then, we attempted to establish CTL lines specific for the epitope I-10(325v) by immunization with dendritic cells pulsed with the peptide, I10(325v) (23). We have successfully generated both a 325(v)-specific CTL line and clones that did not cross-react with the original P18-I10.

Taking advantage of two distinct sets of $CD8^+$ CTL clones specific for either P18-I10 bearing L-type valine or I10(325v) having D-type valine at position 325 presented by the same MHC molecules D^d, we attempted to study the three-dimensional (3D) structural analysis on TCRs and peptide/MHC complexes. Here, using molecular modeling analysis, we would like to show that the critical amino acids for interacting with P18-I10 in determining epitope specificity appear to be the peptide DMSHET within CDR1 of Vβ7, whereas those for interacting with I10(325v) appear to be TNSHNY within CDR1 of Vβ8.3.

MATERIALS AND METHODS

Mice

Female BALB/c (H-2^d) mice were purchased from Charles-River Japan Inc. (Tokyo, Japan). The mice were 6 to 10 weeks of age and were maintained in a specific-pathogen-free environment. All experiments were performed according to the guidelines of the NIH Guide for the Care and Use of Laboratory Animals.

Synthetic peptides

Peptides were synthesized and purified as described previously (24). Table 1 summarizes the peptides used in this study; L-amino acids are represented as capital letters, and D-amino acids as lower-case letters.

Transfectants

BALB/c.3T3 (H-2^d) fibroblast transfectants expressing the HIV-1 gp160 of IIIB isolate (15-12) and control transfectants with selectable marker genes (Neo) (7, 17) were used for the CTL assay. Murine L-cells (H-2^k) transfected with H-$2D^d$ (T4.8.3) (25), H-$2L^d$ (T.1.1.1) (25), and H-$2K^d$ (B4III2) (26) were used to determine the MHC class I restriction of the generated CTL line and clones.

Monoclonal antibodies

We used fluorescein isothiocyanate-conjugated antimouse CD3 (145-2C11), $\alpha\beta$TCR (H57-597), CD4 (RM4-5), and CD8 (53-6.7) monoclonal antibodies (PharMingen, San Diego, CA) to determine the cell surface molecules of the established CTL lines and clones.

CTL lines and clones

The P18-I10-specific CTL line, LINE-IIIB, was generated as described previously (7). Based on a previously reported procedure (23), a CTL line specific for I10(325v) was generated from spleen cells of BALB/c mice immunized with I10(325v)-pulsed splenic dendritic cells. Briefly, immune spleen cells were restimulated in vitro with mitomycin C-treated I10(325v)-pulsed syngeneic BALB/c.3T3 fibroblasts in 24-well culture plates containing 1.5 ml of complete T-cell medium composed of RPMI 1640 medium

TABLE 1 Sequences of substituted peptides used in this study

Peptide	Sequence*															
Residue No.	315										325					329
P18IIIB	R	I	Q	R	G	P	G	R	A	F	V	T	I	G	K	
P18-I10				R	G	P	G	R	A	F	V	T	I			
I10(325I)											I					
I10(325L)											L					
I10(325A)											A					
I10(325Y)											Y					
I10(325F)											F					
I10(325H)											H					
I10(325T)											T					
I10(325S)											S					
I10(325E)											E					
I10(325K)											K					
I10(325R)											R					
I10(325P)											P					
I10(318r)				r												
I10(320p)						p										
I10(322r)								r								
I10(323a)									a							
I10(324f)										f						
I10(325v)											v					
I10(326t)												t				
I10(327i)													i			
I10(325v)				R	G	P	G	R	A	F	v	T	I			
I10(325i)											i					
I10(325l)											l					
I10(325a)											a					
I10(325y)											y					
I10(325f)											f					
I10(325h)											h					
I10(325t)											t					

*Sequences of substituted peptides are derived from and aligned with the sequence of P18-I10, an immunodominant epitope of HIV-1 gp160 envelope glycoprotein of the IIIB strain for the H-2D^d-restricted murine CTL. In these peptides, L-amino acids are expressed as capital letters and corresponding D-amino acids are expressed as small letters.

supplemented with 2 mM L-glutamine, 50 μM 2-ME, 100 U/ml penicillin, 100 μg/ml streptomycin, 10% heat-inactivated FCS, and 10% Rat T-STIM (Collaborative Biomedical Products, Bedford, MA). To establish CTL lines, the generated CTLs were maintained by biweekly stimulation with the mitomycin C-treated I10(325v)-pulsed Neo and were termed LINE-IIIB(325D) cells. CTL clones were established from bulk CTL lines using a limiting dilution technique in 96-well U-bottomed microplates, as described previously (15).

CTL assay

The cytolytic activity of the CTL lines and clones was measured, as previously described (27), using a standard 5-h ^{51}Cr-release assay with various ^{51}Cr-labeled targets, as indicated in the figure legends.

Flow cytometric analysis

Flow cytometric analysis was performed to determine the surface molecule expression of the established CTL lines and clones using a FACScan analyzer (Becton Dickinson Immunochemical Systems, Mountain View, CA). We harvested 5×10^5 cells, washed them twice with serum-free RPMI 1640, and then pelleted them. Fluorescein isothiocyanate-conjugated monoclonal antibodies were added to pellets, and they were then incubated for 30 min at 4°C. Then, the cells were washed three times and resuspended with phosphate-buffered saline (PBS) containing 0.1% bovine serum albumin and 0.1% sodium azide. Dead cells were gated out by forward and side scatter based on propidium iodide uptake. Ten thousand events were acquired for each sample and analyzed using Cell Quest software (Becton Dickinson, Franklin Lakes, NJ).

mRNA extraction, reverse transcription, and PCR amplification

Poly(A) tail-bearing mRNA was isolated from CTL clones using the Fast Track mRNA Isolation Kit (Invitrogen, Carlsbad, CA) according to the manufacturer's instructions. Reverse transcription and PCR amplification of purified mRNA were performed with a GeneAmp RNA PCR Kit (PE Biosystems, Foster City, CA). For the synthesis of T-cell receptor Vβ-specific cDNA, Vβ7-specific primer (ACATCCCTAAAGGATACAGGG) and Vβ8-specific primer (ATATCCCTGATGGGTACAAGG) were used in conjunction with Cβ primer (CCGATGGGAGCACACGAACCCTTAAG). For the synthesis of T-cell receptor Vα-specific cDNA, Vα2-specific primer (AGCAATTCTGAACTGCAGTTA), Vα3-specific primer (CAGCCCGATGCTCGCGTCACT), and Vα16-specific primer (ATGGACTGTGTGTATGAAAC) were used in conjunction with Cα primer (ACTGGACCACAGCCTCAGCGTC).

DNA sequence analysis

PCR products were separated by electrophoresis on a 1% of agarose gel and sliced bands were purified by EASYTRAP glass powder (Takara Bio., Siga, Japan). We then analyzed the purified DNA by a direct-sequence technique, using the ABI PRISM Big Dye Terminator Cycle Sequencing FS Ready Reaction Kit (PE Biosystems), and we analyzed the sequences on the ABI PRISM 377XL DNA Sequencing System (PE Biosystems).

Molecular modeling

Because the actual 3D TCR structures for both Vβ7 and Vβ8.3 were unknown, we carried out comparative and homology modeling to elucidate the spatial relation between TCRβ (Vβ7 or Vβ8.3) and P18-I10 or I10(325v). Comparative modeling predicts the 3D structure of a given protein sequence (target) primarily on the basis of its alignment to one or more proteins of a known 3D structure (templates). It is usually difficult to accurately determine the 3D structure from a protein sequence by theoretical procedures. However, because the 3D TCRβ structure consists of a sandwich comprising a four-stranded antiparallel β-sheet and a three-stranded antiparallel β-sheet that are linked by a disulfide bond, and because the core portion was tightly bound by a hydrogen bond, the 3D structure of the TCRβ, especially the core portion, could be reliably predicted.

Following the above procedure, the so-called threading or 3D template-matching method (28) could be implemented to select templates. For this procedure, we used LIBRA (29) (http://www.ddbj.nig.ac.jp/search/libra_i-e.html) software in which compatible structures of a target sequence are sought from the structural library chosen from the Protein Data Bank (PDB), and the target sequence and 3D profile are aligned by simple dynamic programming. According to the alignment, sequence remounts on the structure and its fitness are evaluated by the pseudoenergy potential. The scores are then sorted from the best-matched templates and shown along with their alignments. Based on the obtained alignments between the template and the target Vβ sequence, a 3D model is calculated by the MODELLER software (30–33), by which five 3D models were obtained from five templates used.

To examine the interaction between the calculated TCR and P18-I10, TCR/peptide/class I MHC complex (PDB code 1kj2) was used for two reasons. First, the 3D structure of the MHC part of 1kj2 is almost identical to that of MHC used in our experiment, which is also resolved (code 1bii) and shows a H-2D^d class I MHC molecule presenting the HIV-derived peptide

P18-I10 (RGPGRAFVTI) (34). The amino acid sequence identity between 1kj2 and 1bii is ~90%. Second, 1kj2 is a TCR/peptide/MHC complex (5), whereas 1bii is only a peptide/MHC complex. In our 3D models, Vβ7 or Vβ8.3 was fitted to the TCRβ position in 1kj2 and was drawn by Mol Feat software (FiatLux, Tokyo, Japan).

Quantum chemical calculation

To study the effect of electric charge on the TCR recognition response, we calculated both the electronic state of P18-I10 and any changes therein based on a single amino acid substitution (325V with 325T) within the P18-I10 using the PM5 molecular orbital method (MOPAC2002) (35). In this calculation, hydrogen atoms were first added to the PDB 3D structures, and then the net charges of all atoms in them were obtained, with the PDB 3D structure being maintained.

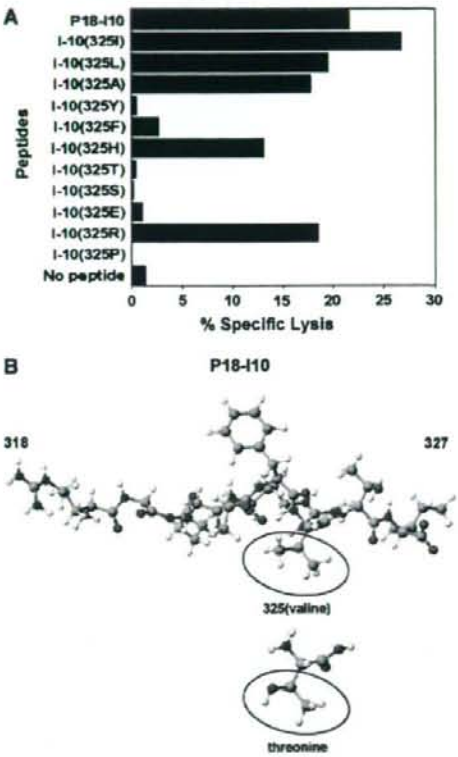

FIGURE 1 Effect of a single amino acid substitution at position 325 within P18-I10 on LINE-IIIB recognition. (*A*) Ten thousand of P18-I10-specific CTL line (LINE-IIIB cells) were added to 5000 ^{51}Cr-labeled BALB/c.3T3 fibroblast target cells in the presence of 3 μM of the substituted peptides at position 325 within P18IIIB, as shown in Table 1. Standard errors of the means of triplicate cultures were <5% of the mean in each case. Results are representative of three independent experiments. (*B*) Ball-and-stick model of peptide P18-I10. The amino acid side chain containing the valine (V) at position 325 within P18-I10 and threonine (T) are shown in the circle. Carbon, oxygen, nitrogen, and hydrogen are shown in gray, red, blue, and white, respectively.

RESULTS

Effect of a single amino acid substitution at position 325 within P18-I10 on LINE-IIIB recognition

First, to see the effect of a single amino acid substitution at position 325 where epitope specificity for LINE-IIIB recognition is determined, a series of P18-I10-derived peptides shown in Table 1 have been synthesized. Similar to our previous findings (10), we confirmed that LINE-IIIB cross-reacted with an aliphatic residue, such as I, L, or A at position 325, in addition to reacting with the original residue V. Moreover, LINE-IIIB cross-reacted with positively charged residues such as R and H but not with the negatively charged E or the uncharged T, S, or P at position 325 (Fig. 1 *A*). Here, we should focus on the case of T, because the 3D structure of the side chain of T is very similar to that of V. When only one carbon atom of the side chain of V is exchanged for one oxygen atom (Fig. 1 *B*; *red*), the amino acid becomes T, except for the hydrogen atoms. According to the quantum chemical calculation using Hamiltonian PM5, the net charge of the carbon atom in V was about $-0.3e$, whereas that of the oxygen atom in T is about $-0.4e$; e represents the elementary charge. This may be the reason why the recognition of V at position 325 by LINE-IIIB was dramatically changed by substitution with T. These results indicate that the charges of the amino acids within the epitope may affect the interaction between TCRs and peptide/MHC complexes.

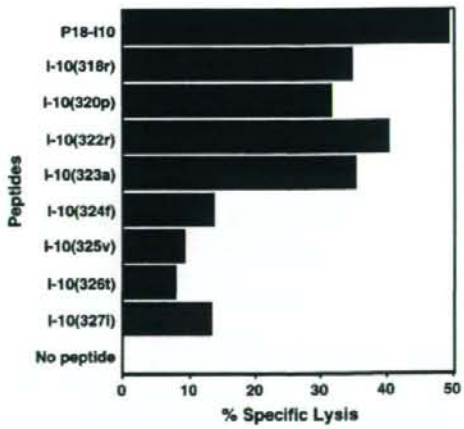

FIGURE 2 Effect of a single amino acid substitution with D-amino acid within an epitope peptide, P18-I10, on LINE-IIIB recognition. Ten thousand LINE-IIIB cells were added to 5000 ^{51}Cr-labeled BALB/c.3T3 fibroblast target cells in the presence of 3 μM of the substituted peptides with a single amino acid substitution by D-amino acid at each corresponding site (represented by lower-case letters in Table 1). Standard errors of the means of triplicate cultures were <5% of the mean in each case. Each experiment was performed at least three times.

Effect of a single amino acid substitution with D-amino acid within an epitope peptide, P18-I10, on LINE-IIIB recognition

Second, to examine the effect of amino acid substitution with the same weight and charged D-amino acid on LINE-IIIB recognition, a series of P18-I10-derived peptides with a single amino acid substitution by D-amino acid at each corresponding site represented by small letters in Table 1 has also been synthesized. When the corresponding D-amino acid was substituted at position 324, 325, 326, or 327, the cytotoxic activity of LINE-IIIB was markedly reduced when compared with other substituted peptides (Fig. 2). This finding suggests that CTL-TCRs can strictly recognize each amino acid within the C-terminal half of the epitope peptide, including at position 325, which is critical for determining epitope specificity, and this is in contrast to their poor ability to recognize each amino acid within the N-terminal half.

Induction of CTL line and clones specific for L-valine or D-valine at position 325 within P18-I10

Then, to study the detailed molecular interactions in determining T-cell specificity, we attempted to generate a CTL line specific for I10(325v) having a single D-type amino acid substitution in P18-I10 at position 325 using immunization of BALB/c mice with syngeneic splenic dendritic cells pulsed with the peptide (23). The I10(325v)-specific CTL line, LINE-IIIB(325D), was successfully established. Although LINE-IIIB(325D) showed some cross-reactivity to P18-I10 in a dose-dependent manner, it was highly specific for I10(325v) (Fig. 3 *A*). Similarly, LINE-IIIB had some cross-reactivity to I10(325v)-sensitized targets (Fig. 3 *B*).

Using limiting dilution techniques described elsewhere (17), we successfully established two clones, IIE11(D) and IIA4(D), predominantly specific for I10(325v) but not for P18-I10 from LINE-IIIB(325D) cells (Fig. 3 *C*) as well as two P18-I10-specific CTL clones, IIH7(L) and IB9(L), from the LINE-IIIB cells (Fig. 3 *D*). Thus, we had established four highly specific clones, two of which were specific for the D-type of valine (v), and the other two for the L-type of valine (V) at position 325 within P18-I10.

Specificity and characterization of the established CTL clones

We further examined the fine specificities of the CTL clones using a series of substituted peptides, each with a single amino acid substitution of either the L- or D-type having an aliphatic or aromatic structure at position 325 in P18-I10 (Table 1).

Among the D-specific clones, IIE11(D) did not cross-react with I10(325I) at all and was strictly specific for the D-type

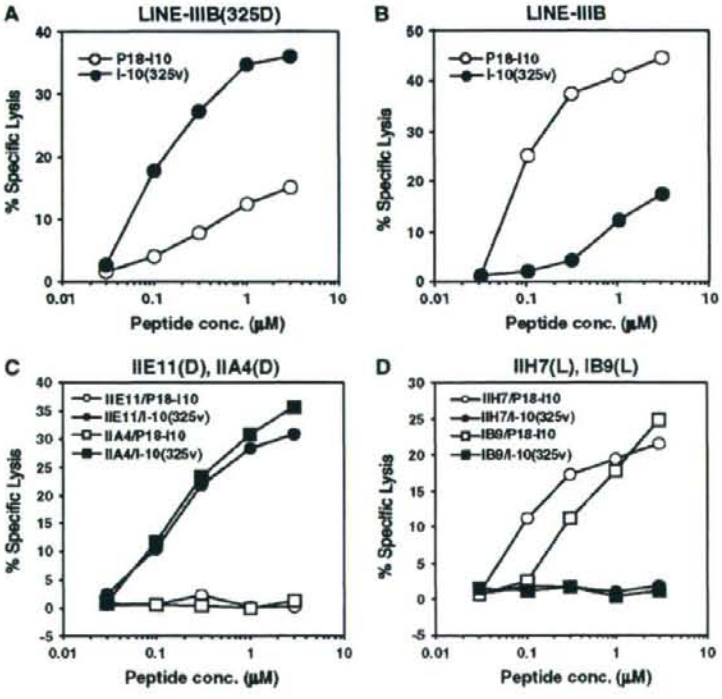

FIGURE 3 Comparison of specificity of the newly established CTL lines and clones against two peptides, peptide P18-I10 and I10(325v). We examined the cytolytic activity of the following distinct CTL lines and clones using a 5-h ^{51}Cr-release assay. To test the peptide specificity, effector cells and ^{51}Cr-labeled BALB/c.3T3 fibroblast targets (E/T ratio was 10:1) were incubated in the presence of various concentrations of either P18-I10 or I10(325v). (*A*) LINE-IIIB(325D) specific for I10(325v) was used for effector cells. (*B*) LINE-IIIB specific for P18-I10 was used for effector cells. (*C*) The CTL clones, IIE11(D) and IIA4(D), derived from LINE-IIIB(325D) were used as effector cells. (*D*) The CTL clones, IIH7(L) and IB9(L), from LINE-IIIB were used as effector cells. Standard errors of the means of triplicate cultures were <5% of the mean in each case. Each experiment was performed at least three times.

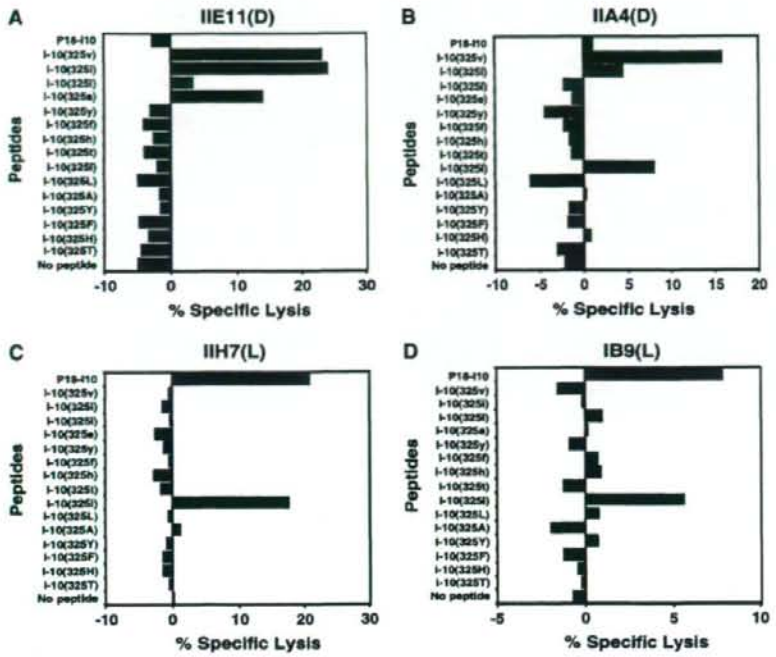

FIGURE 4 Effects of a single amino acid substitution at position 325 within P18-I10 on target sensitization for CTL recognition. We measured the cytolytic activity of the CTL lines and clones using a 5-h ^{51}Cr-release assay. For the analysis of fine peptide specificity, effector cells and ^{51}Cr-labeled BALB/c.3T3 fibroblast targets were mixed with 10 μM of each substituted peptide. The following four clones were used as effectors (E/T ratio was 20:1): (*A*) clone IIE11(D), (*B*) clone IIA4(D), (*C*) clone IIH7(L), and (*D*) clone IB9(L). Standard errors of the means of triplicate cultures were <5% of the mean in each case. Each experiment was performed at least three times.

substitution such as I10(325i) and I10(325a) as well as for the original I10(325v) (Fig. 4 *A*), whereas IIA4(D) showed a weak cross-reactivity for both types of isoleucine, I10(325I) and I10(325i), as well as for the original I10(325v) (Fig. 4 *B*). In addition, both of the L-type-specific CTL clones, IIH7(L) and IB9(L), cross-reacted with I10(325I) as well as with the original P18-I10 (Fig. 4, *C* and *D*). These findings indicate that the CTL clones can specifically distinguish the optical isomers at position 325.

Because P18-I10-specific CTL and their clones are CD8$^+$, D^d-class I MHC molecule-restricted conventional $\alpha\beta$T lymphocytes, we next confirmed the surface molecules and MHC-restriction of the I10(325v)-specific line and clones. LINE-IIIB(325D) and two clones, IIE11(D) and IIA4(D), were all CD3$^+$, CD4$^-$, CD8$^+$, and TCR$\alpha\beta^+$ by FACS analysis (data not shown), and they did not show any cytotoxicity against NK-sensitive YAC-1 cells (data not shown). Moreover, using three L cell (H-2^k) transfectants expressing the class I MHC of the d-haplotype, T4.8.3 (D^d), T1.1.1 (L^d), and B4II2 (K^d) (25,26), we confirmed that the I10(325v)-specific CTL line and clones were restricted by the D^d class I MHC molecule (data not shown).

TCR-sequences of the established clones

Taken together, the two groups of CTL clones with high specificity to the substituted P18-I10-derived peptides, having either the L-type of valine (V) or D-type of valine (v) at position 325, expressed both CD8 and $\alpha\beta$ TCRs, and were restricted by the same class I MHC molecule, D^d. Therefore, taking advantage of the unique combinations of CTL clones, we attempted to perform a precise analysis of the interaction between the TCRs of those clones and the amino acid at

	TCRα chain			
CTL clones	Vα	N	Jα	
IIE11(D)	CAMR	EAD	SNYQLIWGSGTKLIIKPD	Vα16-Jα18BBM142
IIA4(D)	CAMR	EAD	SNYQLIWGSGTKLIIKPD	Vα16-Jα18BBM142
IIH7(L)	CALS	ED	SNYQLIWGSGTKLIIKPD	Vα3-Jα18BBM142
IB9(L)	CAAS	D	SNYQLIWGSGTKLIIKPD	Vα2-Jα18BBM142

	TCRβ chain			
CTL clones	Vβ	N-D-N	Jβ	
IIE11(D)	CASS	DWGGS	TGQLYFGEGSKLTVL	Vβ8.3-Jβ2.2
IIA4(D)	CASS	DWGGS	TGQLYFGEGSKLTVL	Vβ8.3-Jβ2.2
IIH7(L)	CASS	LGYT	EVFFGKGTRLTVV	Vβ7-Jβ1.1
IB9(L)	CASS	LGVT	EVFFGKGTRLTVV	Vβ7-Jβ1.1

FIGURE 5 Nucleotide and amino acid sequences that form the V(D)J region of the TCRα and -β chain from the established CTL clones. We analyzed the amino acid sequences of TCRs in two groups of CTL clones with high specificity to substituted P18-I10-derived peptides, having either the D-type of valine (v) (IIE11(D) and IIA4(D)) or the L-type of valine (V) at position 325 (IIH7(L) and IB9(L)) restricted by the same class I MHC molecules, D^d.

position 325 within epitope to determine the specificity by comparing their TCR sequences.

To investigate the actual amino acid sequences of the TCRs in the CTL clones, we extracted their mRNA and analyzed the nucleotide sequences of the α- and β-chain transcripts after a cDNA synthesis and PCR amplifications. The Vα usage of the I10(325v)-specific clones, IIE11(D) and IIA4(D), were both Vα16 (36), whereas that of the P18-I10-specific clones, IIH7(L) and IB9(L), were Vα3 (37) and Vα2 (BLASTN Accession U88296), respectively (Fig. 5). It should be noted that all of the four distinct clones used the same uncommon Jα gene segment, 18BBM142, determined from a murine alloreactive T-cell hybridoma specific for I-A^{bm12} (38). In contrast, the Vβ usage of the 325(v)-specific clones, IIE11(D) and IIA4(D), was Vβ8.3 (39) with the Jβ 2.2 segment (40) bearing the same CDR3, "DWGGS," whereas the Vβ usage of the 325(L)-specific clones, IIH7 and IB9, was Vβ7 with the Jβ1.1 segment (41) encoding a distinct sequence, "LGYT" and "LGVT," respectively, in the CDR3 flap (Fig. 5). These results strongly indicate that the TCRβ chains of those clones may be responsible for the specificity of the epitope.

Identification of the interaction site between the TCRs and a critical amino acid at position 325 to determine epitope specificity by molecular modeling analysis

Based on the above findings, we then studied the site that determines the epitope specificity of the TCRβ chain in the CTL clones using a 3D molecular modeling analysis (see Materials and Methods). We used the LIBRA software (29,42) to select five compatible templates with excellent Standardized Scores (SD value) for both Vβ7 and Vβ8.3 (Fig. 6 *A*). Fig. 6 *B* shows the alignment of the five most suitable templates for each TCR.

We then used the MODELLER software (30,31,33) to model the 3D structure of the TCR. First, to confirm the

A

Vβ7

Rk	StrC	Lsr	Lal	Rsc	SD	Rs/N	ID%
1	1a6wH	120	127	-65.6	-4.24	-0.517	22.0
2	1dn0D	217	131	-60.1	-3.73	-0.459	19.1
3	1tcrA	202	128	-58.7	-3.60	-0.459	21.1
4	1ao7D	115	124	-56.6	-3.40	-0.457	15.3
5	1kb5A	115	122	-56.4	-3.38	-0.462	23.0

Vβ8.3

Rk	StrC	Lsr	Lal	Rsc	SD	Rs/N	ID%
1	1hxmB	230	118	-58.1	-4.24	-0.492	13.6
2	1etzB	220	124	-55.4	-3.97	-0.446	12.9
3	1fo0A	114	116	-54.5	-3.88	-0.470	19.0
4	1h5bA	113	110	-53.5	-3.78	-0.453	25.4
5	1d1fL	108	114	-52.6	-3.69	-0.461	19.3

B

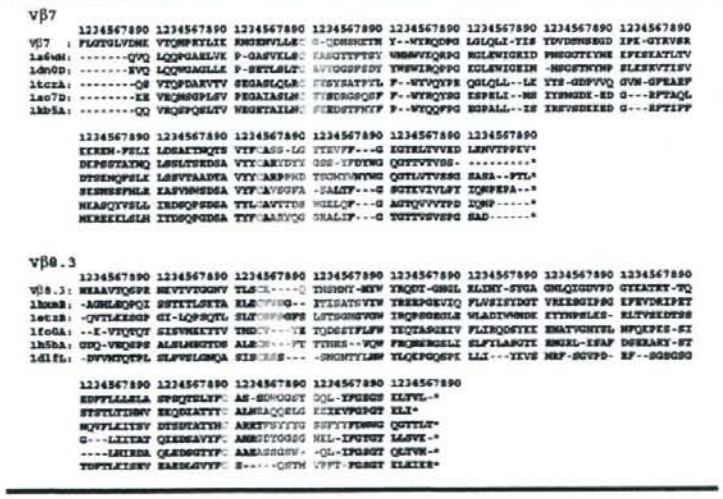

FIGURE 6 (*A*) Compatible templates with excellent Standardized Scores (SD value) for both Vβ7 and Vβ8.3 selected from the LIBRA software. Bold abbreviations are defined as follows: Rk, rank position; StrC, structural code of PDB (the last character is a subunit name); Lsr, length of the structural template; Lal, length of the aligned region; Rsc, raw score of the structural template; SD, standardized score; Rs/N, raw score (Rsc) normalized by the alignment length (Lal); ID%, sequence identity. (*B*) Sequence alignment of TCR Vβ7, Vβ8.3, and each of the five template proteins (1a6wH, 1dn0D, 1tcrA, 1ao7D, 1kb5A for Vβ7 and 1hxmB, 1etzB, 1fo0A, 1h5bA, 1d1fL for Vβ8.3) obtained from the LIBRA software. In this figure, the amino acid sequences of CDR1 and CDR3 from TCR Vβ7 or Vβ8.3 are drawn in red and green, respectively. In 10 template proteins, the corresponding portion of the CDR1 and CDR3 regions are also drawn in red and green, respectively. Conserved cysteine residues upstream of CDR1 and CDR3 are drawn in magenta. Two or three amino acids between the conserved cysteine residues and CDR1 are drawn in blue (see Discussion).

accuracy of our molecular modeling method, we predicted the 3D structure of a previously analyzed protein using MODELLER and then compared it with the experimental 3D structure obtained from x-ray crystallographic analysis for the same protein. We selected two proteins (PDB cord 1dn0D and 1a6wH) having high scores in Fig. 6 *A* and then calculated the 3D structure of 1dn0D using 1a6wH as a template. As shown in Fig. 7, the 3D structure of 1dn0D obtained from MODELLER was similar to that obtained experimentally, and their core regions were nearly identical. These results suggest that our molecular modeling method could be useful for the structural analysis of unknown TCRs.

We next predicted the 3D structures of TCR Vβ7 and Vβ8.3 and analyzed their interactions with P18-I10. The obtained 3D structures for Vβ7 using the five selected templates were quite similar (Fig. 8, *A–D*) and could be confirmed by rotating the calculated structures from various angles (data not shown). In addition, each obtained 3D structure for Vβ7 was fitted to the TCRβ part in 1kj2 to analyze the interaction with the P18-I10 peptide. Although both the CDR1 (*blue*) and CDR3 (*red*) in Vβ7 appeared to interact with the C-terminal half of P18-I10, the critical site for determining epitope specificity (325V, *bright green*) within P18-I10 was found to be more closely associated with the canonical free bottom portion of CDR1 and not with the CDR3 loop (Fig. 8, *A* and *B*): the CDR3 loop is too far from 325V. However, when the 325V was substituted with 325v (*bright red*), the CDR1 loop of Vβ7 might come in contact with the 325v (Fig. 8, *C* and *D*), which seemed to induce conformational interference between the TCR and I10(325v), and thus, the H-2D^d-restricted peptide I10(325v) would not be recognized by the P18-I10-specific clones, IIH7(L) and IB9(L). These results are consistent with our experimental results and indicate that the CDR1 loop of TCR Vβ7 should be the key site for determining P18-I10 specificity in the interaction with the L-valine at position 325.

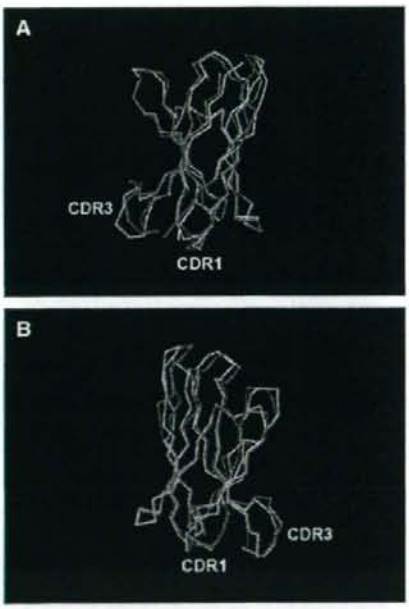

FIGURE 7 Comparison between the predicted 3D structure for 1dn0D by the MODELLER software and that of the same protein registered in PDB. The 3D structure of the protein (PDB cord 1dn0D) was predicted by the MODELLER, a molecular modeling software, using a protein (e.g., PDB cord 1a6wH) as a template. The predicted 3D structure for 1dn0D is drawn in blue, and the PDB 3D structure is drawn in red. Their backbone representations in the molecular modeling are drawn from rotated two distinct views (*A* and *B*).

Similarly, the molecular modeling for Vβ8.3 was performed using another five of the most suitable templates shown in Fig. 6 *A*; each of these actual sequences is shown in Fig. 6 *B*. The calculated 3D structures of Vβ8.3 based on the five templates had almost the same features (Fig. 8, *E–H*) as seen in the case of Vβ7. In contrast to the case of Vβ7, 325v (*bright red*) seemed to be associated with the free bottom portion of the CDR1 loop of Vβ8.3 but not with the CDR3 loop of Vβ8.3 (Fig. 8, *E* and *F*). However, the distance between the 325V (*bright green*) and the CDR1 loop in the case of Vβ8.3 appeared to be greater than that in the case of Vβ7 (Fig. 8, *G* and *H*), which can make a good contact with the 325V in P18-I10.

To substantiate the interaction between valine at position 325 and TCR-CDR1, the distance between terminal atoms in the side chain of amino acids within the epitope peptide and atoms in the main chain of the nearest portion within the TCR was calculated. As shown in Table 2, first to confirm the reliability of our molecular modeling, the distance between the two terminal atoms (OD1 and OD2) in the side chain of the seventh amino acid, aspaltic acid (D), within epitope peptide pKB1(aa: KVITFIDL) and the nearest portion in the TCR from OD1 or OD2 was determined using an already reported TCR/peptide/MHC complex, 1kj2 (PDBcode) obtained from x-ray crystallographic analysis (5). Based on the above observation, the distance between the two terminal atoms (CG1 and CG2) in the side chain of 325V or 325v and their surrounding atoms in the main chain of the obtained TCRs, Vβ7 and Vβ8.3, calculated (Tables 3 and 4) and compared with that of 1kj2. The results indicate that the distance between 325V and CDR1 in Vβ7 is similar to the distance in the case of 1kj2, whereas the distance between 325v and CDR1 in Vβ7 is too small, which may induce conformational interference between them. In contrast, the distance between 325v and CDR1 in Vβ8.3 is similar to 1kj2, but the distance between the 325V and the CDR1 in Vβ8.3 appeared to be too far from that of 1kj2. These results again agreed with our experimental results that Vβ8.3 recognized the epitope I10(325v) having D-valine at position 325 via CDR1 but did not recognize the P18-I10 containing L-valine at that position.

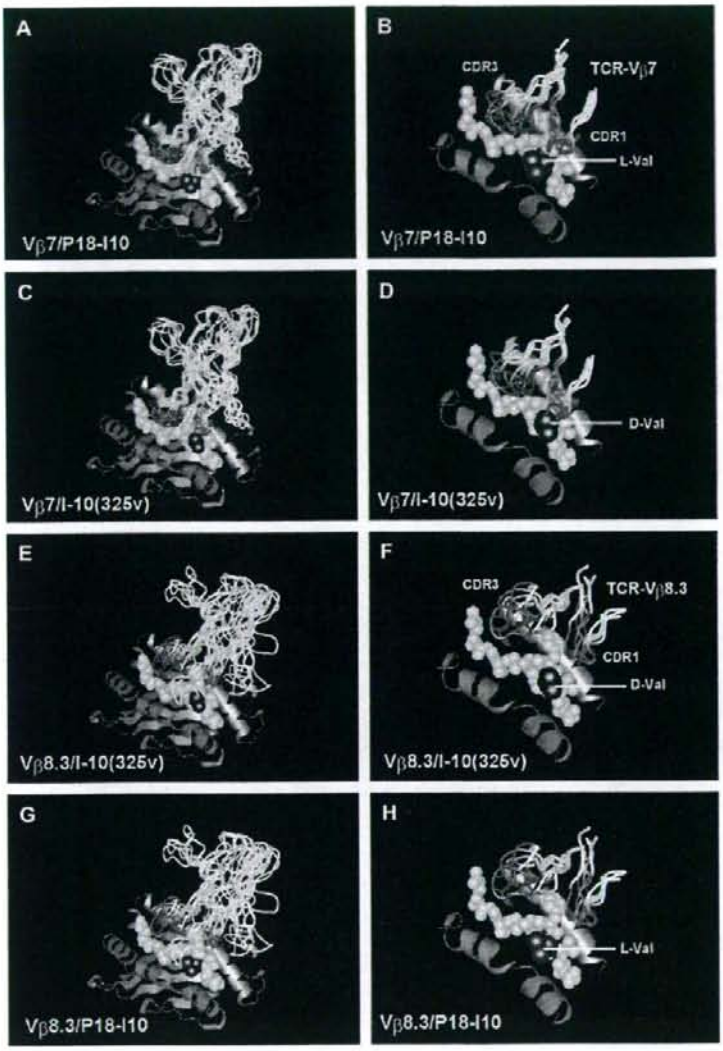

FIGURE 8 3D structures representing the interaction between TCR Vβ7 (Vβ8.3) and P18-I10/H-2D^d Complex or the interaction between TCR Vβ7 (Vβ8.3) and I10(325v)/H-2D^d complex. (*A–H*) The ternary complex of TCR Vβ7 or Vβ8.3 onto either P18-I10 or I10(325v) bounded to the H-2D^d class I MHC molecules were illustrated by computer-based molecular modeling (see Materials and Methods). Horizontal gray backbone represents the H-2D^d class I MHC molecule, and the yellow ball format indicates the D^d-bounded epitope peptide P18-I10. Vertical overlapping white backbones indicate either TCR Vβ7 or Vβ8.3. In these figures, Vβ7 and Vβ8.3 made from five distinct template proteins were overlaid in one figure. The CDR1 and CDR3 loops from both TCR Vβ chains are drawn in cyan and red, respectively. The L-type of valine (V) and the D-type of valine (v) at position 325, where epitope specificity appears to be determined, are shown in bright green and bright red, respectively. The 3D-structures of the (*A*) Vβ7 /H-2D^d/P18-I10, (*B*) enlarged figure of *A*, (*C*) Vβ7 /H-2D^d/I10(325v), (*D*) enlarged figure of *C*, (*E*) Vβ8.3 /H-2D^d/I10(325v), (*F*) enlarged figure of *E*, (*G*) Vβ8.3/H-2D^d/P18-I10, and (*H*) enlarged figure of *G* are shown in eight independent panels.

Therefore, CDR1, but not the CDR3 loop, in Vβ7 or Vβ8.3 seems to play an important role in the recognition of each specific epitope peptide. Moreover, amino acids at positions 26 to 31: DMSHET within the CDR1 of Vβ7, or TNSHNY within the CDR1 of Vβ8.3, appear to interact with the critical amino acid at position 325 to determine the epitope specificity.

DISCUSSION

In our previous study, we found that the amino acids at positions 322R and 324F were critical for D^d binding, and those at position 325V were essential for interacting with TCRs (8,17). Also, the C-terminus 327I appears to be a key amino acid for D^d binding to form the D^d-binding motif (8,18). In this study, we demonstrated that the substitution of a positively charged 322R by 322r did not result in measurable changes in target sensitization, although in our previous study the substitution with uncharged alanine (A) completely eliminated the capacity to sensitize the targets (17), indicating that a positive electric charge must be critical for D^d binding at position 322, and that a reduction of charge in the amino acid might diminish the epitope potency for T-cell activation. As shown in Fig. 1 *B*, the side chains of V and T have the same 3D